Gas-Phase NMR Spectroscopy

CYNTHIA J. JAMESON

Department of Chemistry, M/C-111 University of Illinois at Chicago, Chicago, Illinois 60680

Received April 18, 1991 (Revised Manuscript Received July 25, 1991)

Contents

Cynthia Juan Jameson was born and raised in the Philippines where she did her undergraduate studies. Her Ph.D. research was done under the direction of H. S. Gutowsky at the University of Illinois at Urbana—Champaign. She joined the faculty of the University of Illinois at Chicago in 1968 as an assistant professor and became full professor in 1976. Besides the topics in this review, her interests include molecular electronic property surfaces, intermolecular interaction spectroscopy, nonlinear optical properties, and low-dimensional systems. She is currently a visiting scientist at the National Science Foundation as Program Officer in Experimental Physical Chemistry.

I. Introduction

A nuclear moment is a very sensitive site-specific probe of electronic environment and of dynamics in the gas, liquid, and solid phase. We consider here the nature of the unique information which can be obtained in the gas phase and show that it is possible to make direct connections with theoretical calculations.

Comparison with theoretical calculations necessitates experimental measurements of quantities under conditions as close as possible to that which calculations can mimic. For molecular electronic properties of the isolated molecule this means the zero-pressure limit, and for dynamic quantities such as collision cross sections for chemical reactions or angular momentum transfer, or intermolecular vibrational energy transfer this means the binary collision regime down to the zero-pressure limit. Thus, the gas phase offers up answers to a different set of questions than is normally asked of NMR spectroscopy in condensed phases. There are limitations and advantages.

Some practical limitations are sample volatility, sensitivity, and natural line widths which limit the range of densities and temperatures for the study. For example, ring-inversion studies of cyclohexane at 249 K had to be conducted in samples prepared at pressures in the range 1.1 to 7.6 Torr at 298 K because of condensation of liquid cyclohexane at the high end and the too broad line widths at the low end. Relaxation mechanisms and times in gases are typically such that many intramolecular or intermolecular polarization transfer schemes which are routinely used in condensed phase usually cannot be used here.

Some advantages are the following: (1) Variable-temperature studies can be carried out; density is a variable which is independent of temperature. (2) Intermolecular effects are not eliminated completely but can be significantly reduced relative to the condensed phase. Factors (such as solvent viscosity, bulk magnetic susceptibility, etc.) which are extrinsic to the desired quantities either have no role to play in the gas phase or have significantly reduced and well-defined contributions. This also means that gas data can be compared with data from condensed phase to obtain a

0009-2665/91/0791-1375$09.50/0

measure of solvent effects. (3) One can work in a regime where only two-body effects are important and these can be treated in a quantitative well-defined way. In the linear density region a second virial coefficient for shielding, $\sigma_1(T)$ can be defined. In the linear pressure region experiments can provide collision cross sections for various dynamic processes, and these can be related to theoretical dynamics calculations via quantities such as collision-induced molecular reorientation and rotational energy transfer cross sections and also collision cross sections for intermolecular vibrational energy transfer. (4) One can extrapolate the measured quantities to the zero-density limit to obtain molecular properties (such as chemical shifts) of the isolated molecule or collisionless intramolecular vibrational redistribution (IVR) information. The measured chemical shifts and coupling constants extrapolated to the zero-pressure limit yield quantities that are much closer to those that can be calculated for an isolated molecule, and are the quantities that would be measured in a molecular beam, except that an average over populations of rovibrational states is obtained in the gas. At this limit the intrinsic rate that an energized molecule in the absence of collisions undergoes a unimolecular reaction (e.g., ring inversion) can be obtained.

Gas-phase studies which are reviewed here span a density range of 10^{16} to 10^{21} molecule cm^{-3}, pressures from 1 Torr to 50 atm. Samples studied in subatmospheric pressures can be contained in large diameter tubes, typically 12 mm o.d., 3-cm long or even shorter (1.7 cm), to confine the sample to the active volume region inside the probe in order to minimize effects of diffusion of molecules outside the active volume, a serious concern in these densities where the mean free paths are long. Samples of 5–40 amagat are typically in small diameter tubes (2.2 mm i.d., just under 4 mm o.d.) that can safely withstand pressures of 50 atm over the entire temperature range (NMR measurements reported here are typically in the range 200–400 K, but also up to 550 K). Although diffusion of molecules outside the active volume is not a problem at these densities, sample tubes are kept short to maintain uniform temperature throughout the gas. Commercial spectrometers used for solution studies can be used for gas-phase work; no spectrometer modifications are required. For samples at subatmospheric pressures, larger volume probes allow studies at even lower densities; 12-mm and 20-mm probes have been used.

There was an earlier review of NMR in the gas phase by G. Govil (1973).[1] A review of the effects of intermolecular interactions and intramolecular dynamics on NMR chemical shifts drew from experiments in the gas phase,[2] and NMR relaxation studies in the gas phase were reviewed by Armstrong in 1987.[3]

II. Nuclear Magnetic Shielding

While closely identified with the NMR technique, nuclear magnetic shielding is a molecular electronic property in the same class as other second-order molecular properties such as magnetizability and electric dipole polarizability and is interesting in its own right. Differences between nuclear magnetic shieldings, NMR chemical shifts, are usually quoted with respect to a particular convenient reference liquid for each nucleus. By definition, the nuclear magnetic shielding is an absolute measure of the chemical shift of a nuclear moment, that is, the electronic contribution to the apparent magnetic moment of a nucleus in a specific chemical environment. Its value to the chemist is precisely this, that it is a molecular electronic property which is sensitive to the entire electronic distribution in a molecule but is unique to each unique nuclear site in the molecule, (as is the electric field gradient at a nucleus) rather than an overall property of the entire molecule as is electric dipole polarizability or magnetizability. The sensitivity of the nuclear magnetic shielding to the entire electron distribution of a molecule placed in a magnetic field depends on the extent to which the local magnetic-field-induced current densities are weighted by the inverse cube dependence on the distance from the nucleus in question. It is this which varies substantially from one atom to another in the periodic table more so than from one chemical environment to another of the same atom in different molecules. Thus, the sensitivity of the nuclear magnetic shielding varies with the atomic number of the nucleus, as the $\langle r^{-3}\rangle_{np}$ or $\langle r^{-3}\rangle_{nd}$ for the valence p or d electron of the isolated atom varies with location in the periodic table.[4] Fortunately these $\langle r^{-3}\rangle$ values are experimentally available from electron spin-electron orbit interaction constants. Indeed, the range of chemical shifts observed for each nucleus has been found to have the same periodic behavior with atomic number as does $\langle r^{-3}\rangle$.[5]

In a gas of modest density, the nuclear magnetic shielding σ, like other electronic properties, can be expressed in terms of a virial expansion in density ρ:[6]

$$\sigma(T,\rho) = \sigma_0(T) + \sigma_1(T)\rho + \sigma_2(T)\rho^2 + \ldots \quad (1)$$

The nuclear magnetic shielding of the isolated molecule is $\sigma_0(T)$. In analogy with the second virial coefficient $B(T)$ in the expansion of PV/RT, $\sigma_1(T)$ is called the second virial coefficient of shielding. The density-dependent terms, $\sigma_1(T)\rho + \sigma_2(T)\rho^2 + \ldots$, are due to intermolecular interactions, whereas $\sigma_0(T)$ depends on intramolecular dynamics (rotation and vibration). $\sigma_1(T)$ is a measure of the extent to which shielding is affected by pairwise interactions between molecules. Both $\sigma_0(T)$ and $\sigma_1(T)$ can be obtained from experiments in the gas phase. In a mixture of gases, $\sigma_1(T)$ due to A–A collisions and $\sigma_1(T)$ due to A–B collisions can be separately determined in a series of experiments.

A. Intermolecular Effects

In this section, we assume that bulk susceptibility effects have been corrected for, so that only true intermolecular effects remain. The sign of the intermolecular shielding effects has been found to be universally negative, i.e., deshielding, or

$$[\sigma(T,\rho) - \sigma_0(T)] < 0$$

the known exception being nitrogen in nitriles, pyridine, or other similar sites involving $n\rightarrow\pi^*$ excited states.[7]

1. Second Virial Coefficient of Nuclear Shielding

The nuclear resonance frequency in a pure gas at a given temperature exhibits a linear dependence on density for moderate densities (up to 50 amagat). Figure 1 shows the density dependence of the resonance frequency from the zero-pressure limit all the way up

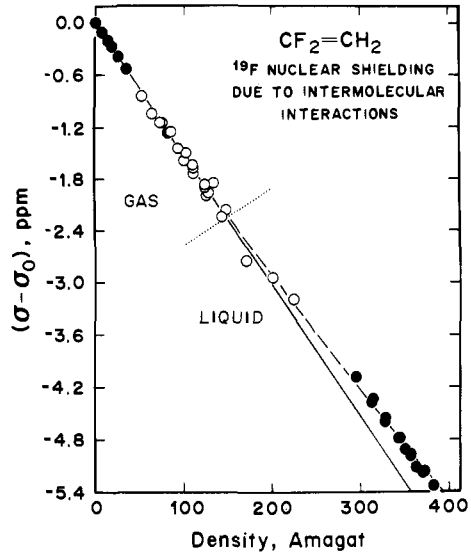

Figure 1. The density dependence of the ^{19}F nuclear shielding in $CF_2=CH_2$. The critical point is 303.3 K and 146 amagat. Open circles and filled circles correspond to independent measurements from two laboratories (reprinted from ref 8; copyright 1984 American Institute of Physics).

to the compressed liquid, for the case of ^{19}F in $CF_2=CH_2$.[8] Operationally, $\sigma_1(T)$ is obtained as follows:

$$\sigma_1(T) = -(1/\nu_0) \lim_{\rho \to 0} (\partial \nu / \partial \rho)_T \qquad (2)$$

and is usually expressed in ppm amagat^{-1} where 1 amagat = 2.687×10^{19} molecules cm^{-3}, the density of an ideal gas at 1 atm and 0 °C. The most extensive information is on ^{19}F shielding, for which $\sigma_1(T)$ data are available in a large number of molecules, given in Table I.[8-17]

It has been noted previously that the range of values of σ_1 for various nuclei roughly correlates with the chemical shift range of the nucleus,[2] being largest for ^{129}Xe[18-23] and smallest for ^1H.[24,25] This is only to be expected. For the reasons mentioned above, the sensitivity of the shielding of a given nucleus to intermolecular effects is expected to be roughly related to $\langle r^{-3} \rangle_{np}$ of the free atom.

The accessibility of the nucleus to the collision partner is also important. The site factors have been incorporated into the binary collision model of Raynes, Buckingham, and Bernstein[27] for nuclei sited at a distance d from the center of mass of the molecule by averaging over all rotational orientations.[28,29] An interesting example of this nuclear site effect is in the density dependence of the isotope effect on deuterium shielding in D_2 and DH in the gas phase. Beckett and Carr's measured values of $[\sigma(D_2) - \sigma(DH)]$ were found to have a linear density dependence.[26] The observed linear density dependence of the isotope shift can be interpreted in terms of the difference in the second virial coefficients of shielding: $[\sigma_1(D_2) - \sigma_1(HD)] = (-0.059 \pm 0.026) \times 10^{-4}$ ppm amagat^{-1}. Since all σ_1 are known to be negative, the greater magnitude of σ_1 in D_2 molecule can be explained in terms of the deuterium nucleus being more exposed in D_2 (where it is at a distance $r_0/2$ from the center of mass) compared to HD (where D is $r_0/3$ from the center of mass). An estimate of this quantity, -0.049×10^{-4} ppm amagat^{-1},[15] compares favorably with the observed value. Another interesting set of measurements confirm the nuclear site

TABLE I. Second Virial Coefficient for ^{19}F Nuclear Shielding, σ_1 (300 K) (ppb amagat^{-1}) Corrected for Bulk Susceptibility

molecule	σ_1	ref	molecule	σ_1	ref
CF_4	−8.65 ± 0.3	9	$CF_2=CFH$		
CF_3H	−6.8 ± 0.7	10	(A)[a]	−9.2 ± 0.9	15
CF_3Cl	−15.7 ± 1.8	10	(B)	−16.4 ± 1.2	15
CF_3Br	−21.1 ± 0.6	10	(C)	−16.3 ± 0.9	15
CF_3I	−24 ± 2.1	11	$CF_2=CFCl$		
CF_3CN	−17.2 ± 1	11	(A)	−22.7 ± 1.8	15
CH_3F	−13.7 ± 1.8	12	(B)	−21.1 ± 1.6	15
CH_2F_2	−4.8 ± 1.1	13	(C)	−20.8 ± 1.6	15
CF_2Cl_2	−16.8 ± 1.7	13	$CF_2=CFBr$		
$CFCl_3$	−15.8 ± 1.7 at 350 K	13	(A)	−26.9 ± 2.3	15
			(B)	−22.3 ± 1.7	15
CF_2HCl	−13.6 ± 0.9	13	(C)	−22.2 ± 4.0	15
$CFHCl_2$	−21.6 ± 1.4	13	$CF_2=CFI$		
CF_3CF_3	−16.2 ± 0.8	10	(A)	−55.6 ± 5.0	15
CF_3CF_2Cl	−18.6 ± 1.4 at 340 K	14	(B)	−45.0 ± 5.3	15
			(C)	−43.5 ± 6.1	15
CF_2ClCF_3	−17.6 ± 1.4 at 340 K	14	BF_3	−16.2 ± 1.8	9
			COF_2	−17.4 ± 1.4	16
CF_3CH_3	−22.7 ± 1.1 at 340 K	14	SiF_4	−15.8 ± 1	9
			SF_6	−15.6 ± 1.5	9
CF_2HCH_3	−19.5 ± 1.3 at 340 K	14	SeF_6	−31.6 ± 2	17
			TeF_6	−36.5 ± 2	17
$CF_2=CH_2$	−12.9 ± 0.6	8	WF_6	−37.4 ± 2	17
$CF_2=CF_2$	−14.8 ± 1.9	8			

[a] F_A is trans to X, F_B is cis to X, and F_C is gem to X in $F_2C=CFX$.

effect in the series of molecules $F_2C=CFX$, where the ^{19}F σ_1 values for the three inequivalent nuclei in the same molecule correlated linearly with the site factors calculated from the molecular geometry. The linear correlation was observed in each of three molecules (X = Cl, Br, and I).[15]

The observed temperature dependence of σ_1 values has generally been in the direction of decreasing magnitude of σ_1 with increasing temperature, except in the two cases of ^{129}Xe in xenon interacting with CO and N_2 molecules.[22] Systems with large magnitudes of σ_1 tend to have a large change of σ_1 with temperature.[2]

2. The Intermolecular Shielding Function

The magnitude of $\sigma_1(T)$ is a measure of the extent to which shielding is affected by pairwise interactions between molecules. For ^{129}Xe in dilute xenon gas, we can explicitly write $\sigma_1(T)$ in terms of the intermolecular potential for Xe–Xe interactions and the nuclear shielding function for a pair of interacting xenon atoms:

$$\sigma_1(T) = \int_0^\infty 4\pi R^2 \, dR[\sigma(R) - \sigma(\infty)] \exp(-V(R)/kT] \qquad (3)$$

$\sigma(\infty)$ is the nuclear shielding of an isolated xenon atom, $\sigma(R)$ is the ^{129}Xe nuclear shielding in xenon dimer at various internuclear separations, and $V(R)$ is the Xe–Xe intermolecular potential. Direct inversion of the $\sigma_1(T)$ data would, in principle, provide the form of the shielding function $\sigma(R)$. This has been done,[30] but the temperature range being limited, the inversion gives only a rough functional form, even with a well-known $V(R)$ function. The form of the intermolecular shielding function found by this direct inversion is only defined in the regions where $\exp[-V(R)/kT]$ is not negligible. Thus, no information can be obtained at R much smaller than R_0 (where V goes to zero). The $\sigma(R)$ function obtained in this way is nonmonotonic: zero

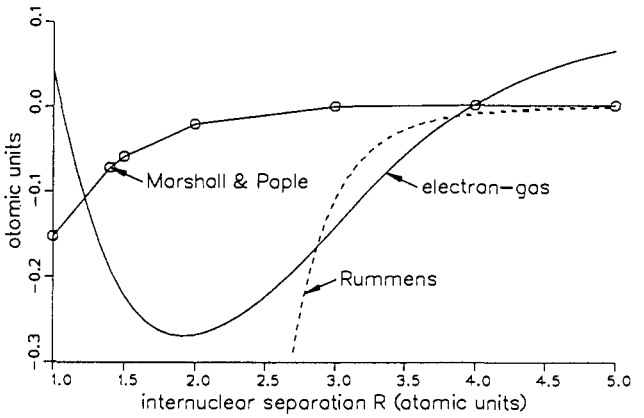

Figure 2. Theoretical calculations of the prototypical intermolecular shielding function, proton shielding in triplet H_2 molecule as a function of internuclear distance (reprinted from ref 35; copyright 1991 Academic Press). The electron gas calculation provides a shielding function that has the same form as the one derived from direct inversion of experimental data for the rare gas pair Xe–Xe.

at large R as it should be, becoming negative in the well region of $V(R)$ and going back to zero at about $R = 0.75R_e$. In the limit $R = 0$ the nuclear shielding should be equal to the diamagnetic shielding of the united atom, a calculable large positive quantity. Thus, the intermolecular shielding function was predicted to be somewhat similar in shape to $V(R)$ itself.

There have been several attempts at calculating $\sigma(R)$ for interacting pairs of molecules. It is well known that the weak long range attractive dispersion forces are not taken into account at all by SCF calculations so that only the shielding changes attributed to short range repulsive interactions can be modeled by any calculation which does not explicitly include correlation effects. The ab initio calculations of $\sigma(R)$ for various systems $(CH_4)_2$, CH_4–He,[31] H_2–He,[32] CO–He,[33] and $(H_2)_2$[34] all have the same behavior, monotonically decreasing as the two molecules approach each other, plunging into large negative values at short R. A recent calculation of the intermolecular shielding function in the prototype of the rare gas pair, triplet H_2, successfully provides the proper behavior,[35] with a minimum in the vicinity of 2 au (see Figure 2). The general long-range behavior of $\sigma(R)$ is thought to be of the form $-3B\alpha_2 I_2 R^{-6}$ [27] or, in a later refinement, $-3B\alpha_2 I_2[I_1/2(I_2 + I_1)]R^{-6}$,[36] with additional orientation-dependent terms for interacting nonmonatomic molecules that necessarily possess nonvanishing electrical moments and, in some cases, anisotropic magnetizabilities.[27] Here, the B parameter is taken to be the same one which is associated with the change in nuclear shielding in an isolated molecule in the presence of a static uniform electric field. Calculations of $\sigma(R)$ using correlated wave functions should soon provide a better description of this function.

3. Many-Body Terms

Nonlinear behavior has been observed at very high densities in xenon gas, for example,[19] where data had been taken over a 250-amagat density range.

The higher order terms in density, taken together, are the opposite sign to the linear term $\sigma_1(T)\rho$. Therefore, while gas-to-liquid shifts are generally deshielding, that is

$$[\sigma(T, \text{liquid}) - \sigma(T, \text{vapor in equilibrium})] < 0$$

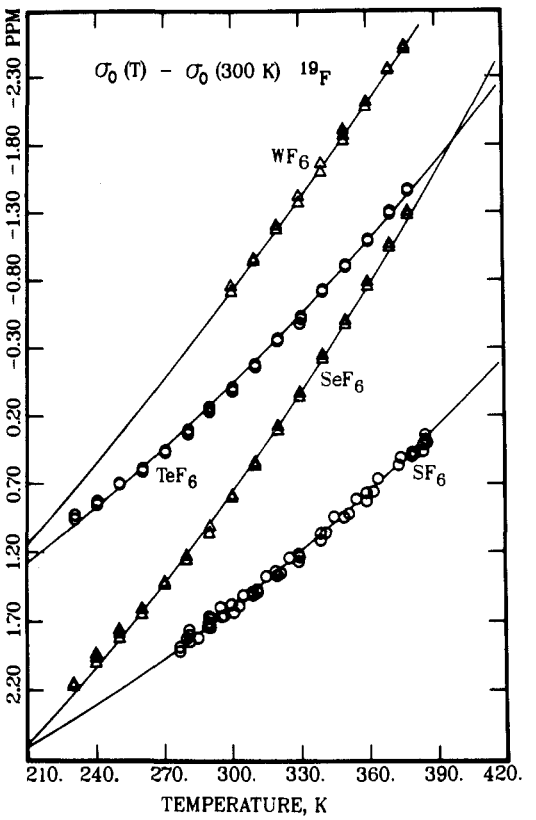

Figure 3. Comparison of the observed temperature dependence $[\sigma_0(T) - \sigma_0(300\text{ K})]$ of ^{19}F in octahedral fluorides with the calculated curves $(\partial\sigma/\partial\Delta r)_e$ $[\langle\Delta r\rangle^T - \langle\Delta r\rangle^{300}]$, using $(\partial\sigma/\partial\Delta r)_e \approx -1930, -2690, -1770$, and -2500 ppm/Å for SF_6, SeF_6, TeF_6, and WF_6, respectively. Except for TeF_6, the individual plots are arbitrarily offset for display (reprinted from ref 37a; copyright 1986 American Institute of Physics).

the gas-to-liquid shift is somewhat smaller than would be expected from the two-body terms alone. An example is shown in Figure 1,[8] where the intermolecular effects have been measured over a 400-amagat range in a favorable case, ^{19}F in $CF_2{=}CH_2$, where the critical point is 303.3 K and 146 amagat.

From gas-to-liquid shifts it is also possible to obtain an "effective $\sigma_1(T)$" which includes many-body terms:[10,16]

$$\frac{[\sigma(T, \text{liquid}) - \sigma(T, \text{vapor in equilibrium})]}{[\rho_{liq} - \rho_{vapor}]_T} = \sigma_{1,eff}(T) \quad (4)$$

In every case this is smaller in absolute value than the $\sigma_1(T)$ value obtained in the low-density gas, a behavior which is clearly shown by the example in Figure 1, that is, the many-body contributions to shielding are the opposite sign to the two-body term.

B. Intramolecular Effects

1. Temperature Dependence of the Nuclear Shielding

In the zero-density limit, the ^{129}Xe shift in xenon gas is independent of temperature, but for a nucleus in any diatomic or polyatomic molecule, there is an observable temperature dependence. Examples are shown in Figure 3.[37a] In practice, the measurements of resonance frequency as a function of density and temperature are carried out, $\sigma_1(T)$ is determined from all data points and then $\sigma_1(T)\rho$ is subtracted from each data point to cor-

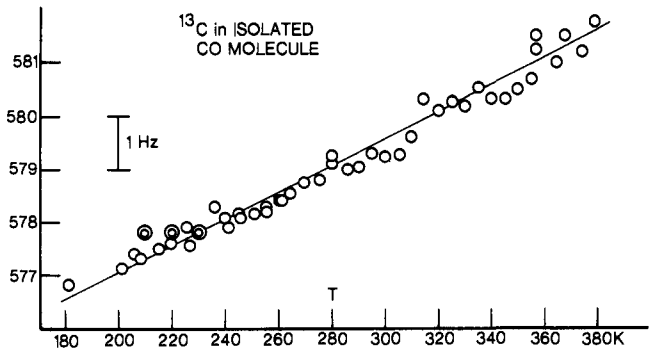

Figure 4. The temperature dependence of ^{13}C shielding in an isolated molecule of CO, measured at 22.633 MHz (reprinted from ref 38; copyright 1981 American Institute of Physics).

rect each one to the zero-density limit. The residual resonance frequencies are then converted to $[\sigma_0(T) - \sigma_0(300\ \mathrm{K})]$, as shown in Figure 3. When the $\sigma_1(T)$ function has been very well characterized, then the residual resonance frequencies are not contaminated with the temperature-dependent intermolecular effects and thus truly reflect the intrinsic temperature dependence of isolated molecules. The general shape of $\sigma_0(T)$ data is shown in Figure 3: deshielding with increasing temperature, with a nonlinear temperature dependence; the curvature is typically as shown here. On the other hand, for a diatomic molecule with a high vibrational frequency, such as CO or N_2, the observed $\sigma_0(T)$ function is linear. See for example Figure 4.[38] The magnitude of the temperature coefficient of shielding depends on the nucleus, roughly dependent on the range of chemical shifts. For a given nucleus it is larger for less shielded environments.

2. Rovibrational Averaging

The temperature dependence of isolated molecules can be interpreted in the context of the Born–Oppenheimer approximation. The separation of electronic and nuclear motion allows an intramolecular potential surface to be defined, which is then used in finding the vibrational functions in terms of nuclear coordinates such as internal coordinates, symmetry coordinates, or normal coordinates. In the same context, a molecular electronic property surface can be defined,[39,40] associated with the same set of nuclear coordinates.[41] Thus, for ^{19}F in MF_6,[37a] the shielding can be expanded in terms of the internal coordinates, Δr_i and $\Delta\alpha_{ij}$:

$$\sigma = \sigma_e + \left(\frac{\partial\sigma}{\partial\Delta r_1}\right)_e \Delta r_1 + \sum_{j=2}^{6}\left(\frac{\partial\sigma}{\partial\Delta r_j}\right)_e \Delta r_j + \frac{1}{2}\left(\frac{\partial^2\sigma}{\partial(\Delta r_1)^2}\right)_e (\Delta r_1)^2 + \ldots \quad (5a)$$

or in terms of normal coordinates Q_i

$$\sigma = \sigma_e + \left(\frac{\partial\sigma}{\partial Q_1}\right)_e Q_1 + \frac{1}{2}\sum_i\sum_j\left(\frac{\partial^2\sigma}{\partial Q_i\partial Q_j}\right)_e Q_iQ_j + \ldots \quad (5b)$$

The thermal average of σ then gives what we have called $\sigma_0(T)$. The averages of the nuclear coordinates can be obtained if the intramolecular force field is available, as they are for SF_6, SeF_6, and TeF_6, for example. For MF_6 molecules,

$$\langle\Delta r\rangle = \frac{1}{\sqrt{6}}\left\{L_{11}\langle Q_1\rangle + \frac{1}{2}\sum_{s=1}^{15}L_1^{ss}\langle Q_s^2\rangle + \ldots\right\} \quad (6)$$

where

$$\langle Q_1^2\rangle = -\frac{1}{4}\left(\frac{h}{4\pi^2c}\right)^{1/2}\omega_1^{-3/2}\sum_{s=1}^{15}\phi_{1ss}\coth\left(\frac{hc\omega_s}{2kT}\right) \quad (7)$$

$$\langle Q_s^2\rangle = \left(\frac{h}{8\pi^2c\omega_s}\right)\coth\left(\frac{hc\omega_s}{2kT}\right) \quad (8)$$

ϕ_{1ss} are cubic force constants in dimensionless normal coordinates, which can be expressed in terms of the **L** tensor elements L_{ij}, L_s^{ss}, etc., the cubic force constants in curvilinear internal coordinates, the quadratic force constants, and the harmonic frequencies ω_s. The coth $(hc\omega_s/2kT)$ is an approximate thermal average of $2\langle v_s + {}^1/_2\rangle$, taken over a harmonic density of states. (See for example ref 37a.) If the approximation is made such that only the $\langle\Delta r\rangle$ term is used to fit the experimental $\sigma_0(T)$ curves, then a single parameter $(\partial\sigma/\partial\Delta r)_e$ can be obtained empirically from the observed temperature dependence. In the examples shown in Figure 3, the curves shown are the calculated curves

$$\sigma_0(T) - \sigma_0(300\ \mathrm{K}) \approx (\partial\sigma/\partial\Delta r)_e[\langle\Delta r\rangle^T - \langle\Delta r\rangle^{300}] \quad (9)$$

using $(\partial\sigma/\partial\Delta r)_e$ = −1930, −2690, −1770, and −2500 ppm/Å for ^{19}F in SF_6, SeF_6, TeF_6, and WF_6, respectively. The sign of $(\partial\sigma/\partial\Delta r)_e$ is commonly negative, although positive signs are known in a few cases.[37b,c] Note that the observed curvature is intrinsic in the temperature dependence of $\langle\Delta r\rangle^T$. The temperature dependence of $\langle(\Delta r)^2\rangle^T$ is likewise made up of linear combinations of coth $(hc\omega_s/2kT)$ terms. Furthermore, a centrifugal stretching (rotational) contribution is added to the vibrational average in eq 6 to obtain the total mean bond displacement $\langle\Delta r\rangle^T$. These data are only good enough to determine a single empirical parameter. Thus, it is not feasible to extract both $(\partial\sigma/\partial\Delta r)_e$ and $(\partial^2\sigma/\partial(\Delta r)^2)_e$ from the data.

For diatomic molecules with very high vibrational frequencies coth $(hc\omega/2kT)$ is very nearly 1.0 and nearly independent of temperature.[39] In that case the observed temperature dependence of $\sigma_0(T)$ is nearly entirely due to the rotational contribution, which is linear with temperature, as is the case for ^{13}C in CO molecule, shown in Figure 4.[38]

A dependence of nuclear shielding on isotopic masses of neighboring nuclei can also be expected from using the same theoretical framework.[42a] For corresponding vibrational quantum numbers the mean value of Δr is smaller for the heavier molecule. As a molecule rotates, all atoms tend to move away from the center of mass but the centrifugal stretching in the molecule with the lighter atoms is greater than in the corresponding isotopomer. Thus, both vibration and rotation contribute to a larger mean bond extension in the lighter isotopomer than in the heavier one. The consequence is that a difference in nuclear shielding will be observed upon isotopic substitution of a neighboring atom in the molecule. This is known as a secondary isotope shift. The same rovibrational analysis provides both the intrinsic temperature dependence observed in the zero-density limit and the isotope shift. The latter, usually observed in condensed phase where the NMR signals

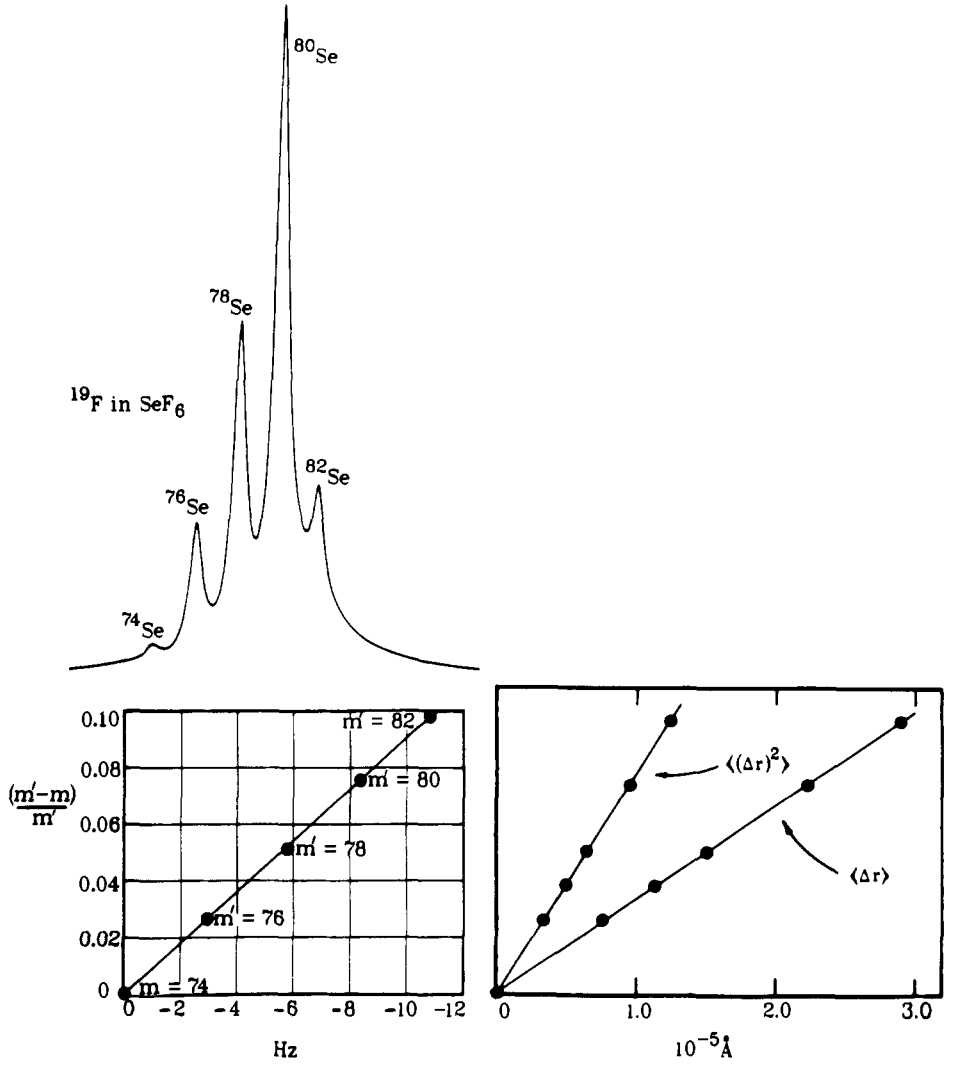

Figure 5. ^{19}F spectrum in liquid SeF_6 at 300 K at 188.3 MHz, showing only the "center peak". The intensities of the peaks for the isotopomers are consistent with the natural abundance of the Se isotopes. The isotope shifts for $^{m'}SeF_6$ and $^{m}SeF_6$ are plotted for $m = 74$. The calculated thermal averages of the mean bond displacement and the mean square amplitudes are shown to have a direct relationship with the same mass factor $(m' - m)/m'$ (reprinted from ref 17; copyright 1986 American Institute of Physics).

are narrower, serves as a check. It is not yet known how large the medium effects on the isotope shift are. Presumably they should be small since both isotopomers are affected by the solvent in nearly the same way, unless the isotopic substitution site is involved in association, e.g., in hydrogen bonding.

The rovibrational calculations in MF_6 molecules reveal a linear relationship of the mass factor $(m' - m)/m'$ with both $\langle \Delta r \rangle^T$ and $\langle (\Delta r)^2 \rangle^T$. This is matched by experiment, as shown by the example in Figure 5[17] where the Se-induced ^{19}F chemical shifts in which m_{Se} is replaced by m'_{Se} are found to have an extraordinarily good straight line when plotted against this mass factor. The assignments are clearly borne out by the relative intensities of the peaks which are seen to be in the ratio of the respective natural abundances of the Se isotopes. Details of the theoretical interpretation of NMR isotope shifts are given elsewhere.[42a]

3. The Intramolecular Shielding Function

The complete interpretation of $\sigma_0(T)$ requires an independent knowledge of the intramolecular shielding function. Intramolecular shielding surfaces have been calculated for ^{13}C and ^{1}H in CH_4,[42b] ^{17}O and ^{1}H in H_2O,[42c] and for several diatomic molecules.[37c] An example of such a surface calculated by us is shown in Figures 6 and 7[43] for ^{15}N in NH_3. The ^{15}N temperature dependence in NH_3 molecule is unusually flat.[43] [In earlier work, some residual temperature dependence of the intermolecular effects had not been completely separated out.] On the other hand, the deuterium-induced isotope shift is of normal sign and magnitude. In this case it would be foolhardy to attempt a fit of the data to one parameter as was possible for ^{19}F systems. Instead, an ab initio ^{15}N shielding surface was calculated by using the LORG method.[44] The intramolecular potential surface was derived from vibrational spectra. In particular, the empirical inversion potential was taken from a fit by Spirko to all the spectral data for several deuterated isotopomers including ^{15}N and ^{14}N.[45,46] A numerical solution of the vibrational equation for the inversion coordinate provided the functions necessary for the proper averaging of the nuclear shielding in each of the symmetric and antisymmetric states. Thermal averages were obtained for both ND_3 and NH_3 by using Boltzmann averaging over these states. The rest of the symmetry coordinates were treated in the conventional way, averaging over small amplitudes. The contribution of the inversion coordinate to the temperature dependence of the ^{15}N

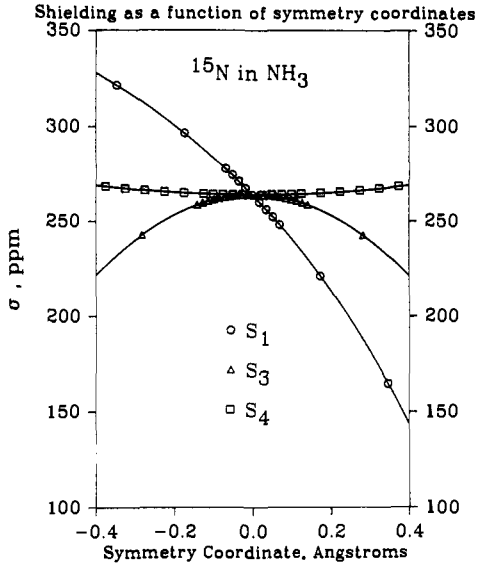

Figure 6. Traces on the ab initio nitrogen magnetic shielding surface of ammonia molecule along the symmetry coordinates corresponding to symmetric stretch (S_1), asymmetric stretch (S_3), and asymmetric bend (S_4), calculated by using the localized orbital local origins method (LORG) of Hansen and Bouman (reprinted from ref 43; copyright 1991 American Institute of Physics).

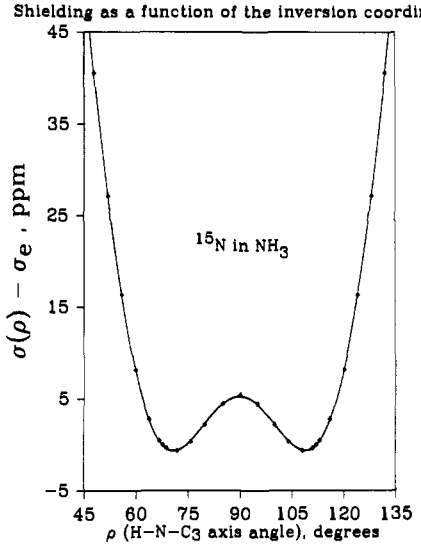

Figure 7. A trace on the ab initio nitrogen shielding surface along the inversion coordinate of ammonia molecule, calculated by using the LORG method (reprinted from ref 43; copyright 1991 American Institute of Physics).

shielding is opposite in sign to that of the rest, leading to an unusually small net temperature dependence. The theoretical $\sigma_0(T)$ function so obtained[43] agrees very well with experiment, and the theoretical isotope shift of 2.36 ppm is in fair agreement with the experimental value, 1.87 ppm.[47]

The theoretical framework for rovibrational averaging appears to be successful in the interpretation of the temperature-dependent shielding in the zero-density limit and in the interpretation of the isotope shift in NMR. Nuclear magnetic shielding serves as a paradigm for molecular electronic properties.[41] Where the data can be obtained with the resolution and precision as in NMR in gas phase, other molecular electronic properties can be investigated in the same way as shown here for shielding. The region of the property surface that contributes significantly to the average is that region corresponding to the deep pocket in the intramolecular potential energy surface, in the immediate vicinity of the equilibrium molecular geometry. The measured temperature dependence in the zero-density limit provides information about the shape of the property surface in this region of molecular geometries. Isotope effects provide differently weighted averages over the same region, thus providing a separate test of the surface.

C. Absolute Shielding

In making a comparison of ab initio calculated values at the equilibrium geometries with experimental chemical shifts, it is necessary to have absolute quantities (shielding values) to compare with rather than differences (chemical shift values). We have already seen that medium effects can be eliminated by making gas-phase measurements extrapolated to the zero-density limit to obtain precise differences $[\sigma_0(300\ \mathrm{K})]_A - [\sigma_0(300\ \mathrm{K})]_B$. To obtain $\sigma_0(300\ \mathrm{K})$ from such differences, one needs an independent measure of $\sigma_0(300\ \mathrm{K})$ for at least *one* molecule for each NMR nucleus. Once this is known, all other $\sigma_0(300\ \mathrm{K})$ can be obtained from the very precise differences. An independent measure of absolute shielding is found by using an identity which relates the paramagnetic part of the shielding tensor to the electronic part of the spin-rotation tensor:[48]

$$\sigma_{xx}^{\mathrm{p}} = \left(\frac{m_{\mathrm{p}}}{m_{\mathrm{e}} 2 g_{\mathrm{N}}}\right)\left(\frac{C_{xx}^{(\mathrm{N})}}{B_{xx}}\right) - \frac{e^2}{2mc^2}\sum_{\mathrm{N}'} Z_{\mathrm{N}'}\left(\frac{y^2+z^2}{R^3}\right)_{\mathrm{NN}'} \quad (10a)$$

where $C_{xx}^{(\mathrm{N})}$ and B_{xx} are the spin-rotation and molecular-rotational constants for the xx principal inertial axis. The last term depends only on the coordinates of all the other nuclei N′ relative to N in the inertial axis system. The isotropic average is then

$$\sigma = \sigma^{\mathrm{d}} + \left(\frac{m_{\mathrm{p}}}{m_{\mathrm{e}} 2 g_{\mathrm{N}}}\right)\left(\frac{1}{3}\right)\sum_{\alpha\alpha}\frac{C_{\alpha\alpha}^{(\mathrm{N})}}{B_{\alpha\alpha}} - \frac{e^2}{3mc^2}\sum_{\mathrm{N}'}\frac{Z_{\mathrm{N}'}}{R_{\mathrm{NN}'}} \quad (10b)$$

The diamagnetic shielding σ^{d} is a first-order electronic property, easily calculated from the ground electronic wave function of the molecule. In any case, the last term, arising from the nuclear part of the spin-rotation interaction, very nearly equals the change in the diamagnetic shielding in going from the free atom to the molecule.[48] Thus, to within a few ppm

$$\sigma \approx \sigma^{\mathrm{d}}\ (\text{free atom}) + \frac{m_{\mathrm{p}}}{m_{\mathrm{e}} 2 g_{\mathrm{N}}}\frac{1}{3}\sum_{\alpha\alpha}\frac{C_{\alpha\alpha}^{(\mathrm{N})}}{B_{\alpha\alpha}}$$

To obtain σ_e from the above relations, one needs to use the spin-rotation values at the equilibrium molecular geometry, necessitating some rovibrational correction of the same type as discussed in the previous section.

The spin-rotation tensor has been used to determine the ^{15}N absolute shielding in NH_3, ^{19}F in HF, ^{13}C in CO, ^{31}P in PH_3, and these absolute shieldings have been used to establish all other absolute shieldings in various molecules containing these nuclei. Gas-phase studies provide the relative differences at the zero-density limit[49-56] and these can be converted to $\sigma_0(300\ \mathrm{K})$ values absolutely. If the commonly used liquid reference is also measured relative to this one molecule, then all past and future measurements of chemical shifts relative to

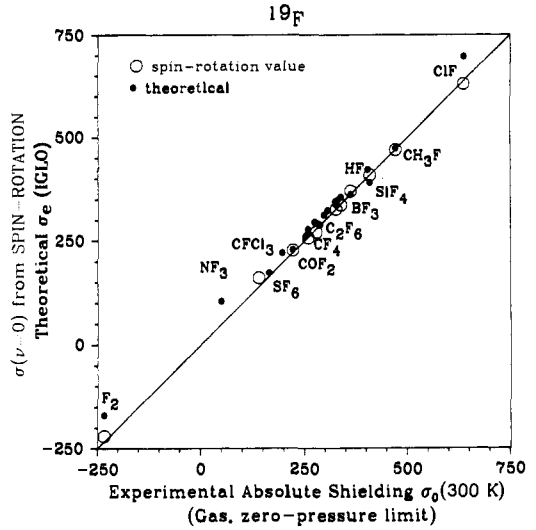

Figure 8. Comparison of experimental absolute shielding values of ^{19}F from gas-phase measurements in the zero-density limit with theoretical values from ab initio calculations of Fleischer and Schindler[67] by the IGLO method. The gas-phase measurements are converted to absolute shielding by using HF as the primary reference molecule. Also shown are the individual absolute shielding values derived from independent measurements of the ^{19}F spin rotation constants in various molecules, compared to the gas phase measurements. Gas-phase experimental values and spin-rotation-derived values are given in ref 50 and 52.

TABLE II. Absolute Shielding for Selected Nuclei from Gas-Phase Experiments, σ_0 (300 K), and Representative ab Initio Theoretical Values of Shielding at the Equilibrium Geometry, σ_e

nucleus	molecule	σ_0(300 K), ppm	ref	σ_e, ppm	ref
^{15}N	N_2	-61.6	51	-72.2	59
	*N*NO	99.5	51	105	58
	N*N*O	11.3	51	6	58
	NH_3	264.54	*a*	264.0	43
	HCN	-20.4	5	-16.98	71
^{17}O	H_2O	344.0	60	336.42	62
	CO_2	243.4	60	223.7	57
	NNO	200.5	60	212	58
	OCS	107.9	60	84.6	61
	CO	-42.3	60	-69.15	71
	OF_2	-473.1	60	-426	66
^{29}Si	SiH_4	475.3	63	479	64
	SiF_4	482	63	488	64
^{31}P	PH_3	594.45	*b*	594	65
	P_4	879.85	*c*	856	65
	PN	53	*d*	67	65
	PMe_3	391.71	53	429.8	66
	OPF_3	363.43	53	384.6	66
	PF_3	222.69	53	255	64
	PCl_3	111.29	53	150	66

[a] Kukolich, S. G. *J. Am. Chem. Soc.* **1975**, *97*, 5704. [b] Davies, P. B.; Neumann, R. M.; Wofsy, S. C.; Klemperer, W. *J. Chem. Phys.* **1971**, *55*, 3564. [c] Heckmann, G.; Fluck, E. *Mol.-Phys.* **1972**, *23*, 175. [d] Raymonda, J.; Klemperer, W. *J. Chem. Phys.* **1971**, *55*, 232.

this liquid reference can be converted to absolute shieldings.

Ab initio theoretical values of shielding at the rigid molecular geometry, σ_e, have been compared directly with the experimental values of σ_0(300 K) from gas-phase studies for ^{13}C[49,56] and other nuclei.[43,51,53,57-66] Examples are given in Table II and in Figure 8.[50,52,67] (For a more complete collection of ab initio calculations and comparisons with experiment, see ref 68.) As we have seen above, rovibrational corrections should be calculated and added to theoretical σ_e before comparing

TABLE III. Magnitudes of Rovibrational Corrections for Selected Molecules

nucleus	molecule	$[\sigma_0(300\ K) - \sigma_e]$, ppm	ref
^{1}H	H_2O	-0.58	69
^{13}C	CO	-2.74	71
	CH_4	-3.6	70
^{15}N	$^{15}NH_3$	-8.81	43
	$^{15}ND_3$	-6.45	43
^{17}O	H_2O	-13.6	69
	CO	-5.56	71
^{19}F	SF_6	-12.0	37a
	HF	-11.2	72
^{31}P	PH_3	-12.78	73
	PD_3	-9.33	73

with the experimental values σ_0(300 K). For some molecules this latter value is not very different from the zero-point vibrational average shielding σ_0(0 K). Similarly, the observed spin-rotation constants should be corrected for rovibrational effects before using the identity expressed in eq 10 to obtain σ_e. Nevertheless, the agreement between absolute shielding values derived from spin rotation constants and those from gas-phase measurements in the zero-pressure limit is remarkably good in Figure 8, as shown by the open circles. This indicates that it should be possible to obtain the isotropic average value of the spin-rotation tensor from NMR chemical shift measurements in the gas phase, which is much easier than obtaining spin-rotation constants from molecular beam magnetic or electric resonance spectroscopy. Representative magnitudes of rovibrational corrections are shown in Table III.[37a,43,69-73]

Better tests of ab initio calculations are provided by the individual tensor components measured in oriented molecules in argon matrix, in clathrates, in polycrystalline solids, or in single crystals. (See a compilation of such data in ref 74.) However, only relative shieldings (chemical shift tensors) can be obtained in these media and there are always intermolecular effects. Thus, gas-phase data are needed to convert these shift tensors to absolute shielding tensors and also to provide a measure of the average intermolecular effects, i.e., the difference between the average shielding obtained in condensed phase and the isotropic average shielding obtained in the zero-density limit.

D. Conclusions

We have found that the nuclear magnetic shielding provides an excellent challenge to the theoretician; there are well-defined, precise experimental quantities to compare with, some requiring theory at the cutting edge. Absolute shielding rather than chemical shift is the appropriate test of theory. Nuclear magnetic shielding is a paradigm for molecular electronic properties. The high resolution and precision obtainable in NMR spectroscopy in the gas phase allows the intermolecular effects to be separated out and examined and for the rovibrational averaging to be accounted for. No other second virial coefficient of a molecular electronic property is as well characterized as σ_1. Theoretical forms of the intermolecular shielding function can be tested by comparison with experiments: the intermolecular shielding function is intimately linked to the intermolecular potential energy surface in the observable temperature-dependent σ_1. Parallel developments in the intermolecular electric dipole polarizability

functions should draw from the $\sigma_1(T)$ example. Intermolecular effects on the electric field gradients at nuclear sites have not yet been systematically studied, although it is well known that the nuclear quadrupole coupling constant changes substantially in going from gas to condensed phases. The magnitudes of σ_1 could serve as guides in estimating the electric field gradient sensitivity to intermolecular effects.

The intramolecular nuclear magnetic shielding surface is a paradigm for molecular electronic property surfaces. The rovibrational effects observed in gas-phase data provide additional stringent tests of theory, independent of the value of the property at the equilibrium molecular geometry. Except for electric dipole moment, no other electronic property surfaces have been so well characterized. For nuclear magnetic shielding, we have shown the relationship between the dependence of an electronic property on the rotational/vibrational states, the way in which the measured temperature dependence in the gas phase and the isotope effects provide tests of both the shielding surface and the intramolecular potential energy surface. The next challenge is that of fluxional molecules. Here the dynamic averaging can no longer be carried out in terms of the small amplitudes describable by a perturbation theory approach or an expansion in powers of the nuclear displacement coordinates described by eq 5–8. The vibrational averaging has to be done directly, as was done for the inversion coordinate in ammonia.

III. Spin Relaxation

Nuclear spin relaxation studies in the gas phase were reviewed in 1987.[3] We will discuss primarily those studies published later.

Spin-relaxation data in the gas phase in the "extreme narrowing" limit provide a stringent test of the anisotropy of an existing intermolecular potential in the same way that virial coefficients, transport properties, and viscosities provide tests of the isotropic part of the potential. In some cases, such as H_2–He,[75,76] spin-relaxation data have been shown to give perhaps the single most powerful test of the anisotropic part of the intermolecular interaction. There are other observables such as the Senftleben–Beenakker effects, depolarized Rayleigh scattering, sound absorption, and pressure broadening of rotational lines in the IR, which are also sensitive to the anisotropy of the potential.[77] These furnish complementary information. Of course, the most detailed information on the anisotropy of a potential can be obtained from comprehensive high-resolution spectral studies of a van der Waals complex such as is now available for HCN–HF.[78] For most van der Waals dimers, however, only limited spectroscopic data are available and these are not usually sufficient to provide the parameters in the angle-dependent part. Where possible, the most detailed experimental information such as state-to-state cross sections provide the best test for comparison with exact close coupling quantum scattering calculations on well-established potential surfaces. For molecules with a small rotational constant, such as those reviewed here, close coupling calculations are not practical, however. These molecules behave nearly classically in the sense that at room temperature a large number of rotational states are occupied and only the vibrational ground state is significantly populated. For such systems, a multiproperty-fitted empirical potential surface can be based on thermal average collision cross sections of various types including those from spin relaxation measurements, together with pressure virial coefficients and molecular beam scattering cross sections, which properties may be treatable at the classical, semiclassical, or IOS level of quantum scattering. Spin relaxation gives cross sections which are due entirely to the angle dependence of the interaction potential. Of the thermal average properties that are directly related to or arise solely from the angle-dependent part of the interaction, those which are related to the reorientation of the rotational angular momentum vector from NMR T_1 measurements in the gas phase are the most promising. Finally, spin-relaxation measurements in the gas phase yield molecular reorientation and rotational energy transfer rates which are of interest in their own right for the interpretation of experiments involving molecular dynamics and energy disposal in the gas phase.

A. The Connection with Intermolecular Potentials. Collision Cross Sections

In that density regime where the frequency of collisions exceeds the nuclear Larmor frequency (the extreme narrowing limit), T_1 has a linear dependence on density ρ so the values of $(T_1/\rho)_{\text{lin,SR}}$, $(T_1/\rho)_{\text{lin,q}}$, $(T_1/\rho)_{\text{lin,d}}$ are the quantities which characterize the molecule and its collision partner, in spin rotation, quadrupolar, and intramolecular dipole–dipole relaxation.

In order to make the connection with intermolecular potential energy surfaces, the relaxation time T_1 has to be expressed in terms of quantities that may be directly calculated once an intermolecular potential energy surface has been supplied. The expressions for the intramolecular relaxation mechanisms, spin rotation, dipolar, and quadrupolar, have been derived by Gordon.[79–81] For example, for a linear molecule in the extreme narrowing limit: (1) The spin-rotation relaxation rate is given by

$$\left(\frac{1}{T_1}\right)_{\text{lin,SR}} = \frac{2\,C^2\langle j(j+1)\rangle}{3\,\rho\bar{v}}[\mathbf{d}^{(1)}\langle\sigma^{(1)}\rangle^{-1}\mathbf{P}\mathbf{d}^{(1)}] \qquad (11)$$

where C is the spin-rotation constant, $\bar{v}$ is the mean relative velocity,

$$d_j^{(1)} = [j(j+1)]^{1/2}\langle j(j+1)\rangle^{-1/2} \qquad (12)$$

and the diagonal matrix $\mathbf{P}$ gives the populations of the initial states normalized such that

$$\mathbf{d}^{(1)}\mathbf{P}\mathbf{d}^{(1)} = 1 \qquad (13)$$

(2) The quadrupolar relaxation rate (for low densities only) is given by

$$\left(\frac{1}{T_1}\right)_{\text{lin,q}} = \frac{3\,(2I+3)}{\rho\bar{v}160I^2(2I-1)}\left(\frac{eqQ}{\hbar}\right)^2[\mathbf{d}^{(2)}\langle\sigma^{(2)}\rangle^{-1}\mathbf{P}\mathbf{d}^{(2)}] \qquad (14)$$

where $(eqQ/\hbar)$ is the nuclear electric quadrupole coupling constant

$$d_j^{(2)} = \left[\frac{j(j+1)}{(2j-1)(2j+3)}\right]^{1/2} \qquad (15)$$

Similarly, the intramolecular dipole–dipole relaxation rate is given by

$$\left(\frac{1}{T_1}\right)_{\text{lin,d}} = \frac{2}{3}\frac{I(I+1)}{\rho\bar{v}}\gamma^4\hbar^2\langle R^{-3}\rangle^2[\mathbf{d}^{(2)}\langle\sigma^{(2)}\rangle^{-1}\mathbf{P}\mathbf{d}^{(2)}] \quad (16)$$

Neilsen and Gordon provide the general formulas for the sigma matrix elements $\langle\sigma^{(1)}\rangle$ and $\langle\sigma^{(2)}\rangle$ which give the effect of an average collision in changing the time development of the tensors, which are respectively the rotational angular momentum vector and the second rank tensor associated with both the quadrupolar interaction and the dipolar interaction. When the sigma matrices are diagonally dominant, eqs 11, 14, and 16 have the form of a weighted average, one term in the sum for each j state. For spin rotation the weights grow faster with j than just population weighting, since the coupling increases with the magnitude of the **J** vector. The spin-rotation relaxation time therefore contains information mainly about the higher j states. On the other hand, the $d_j^{(2)}$ appearing in quadrupolar relaxation are largest for the very low j states, approaching the value $^1/_4$ asymptotically for high j. Thus, the quadrupolar or dipolar relaxation provides complementary information to spin rotation relaxation. Neilsen and Gordon have shown that $\langle\sigma^{(1)}\rangle$ includes contributions from collisions which change the magnitude of the rotational angular momentum as well as those which reorient its direction; $\langle\sigma^{(2)}\rangle$ includes large contributions from reorientation and to a minor extent from changes in j value. Equations analogous to eqs 11 and 16 have been derived by Liu and McCourt using the kinetic theory of gases in the context of the generalized Boltzmann equation.[82]

Equation 11 is the same as that which was derived by using a single-exponential spin correlation function[83]

$$\left(\frac{1}{T_1}\right)_{\text{lin,SR}} = \frac{2}{3}C^2(2I_0kT)\tau_J \quad (17)$$

for a linear molecule. In the gas phase the correlation time τ_J is the average time between collisions that are effective in changing the rotational angular momentum vector, i.e., we can write it as

$$\tau_J = (\rho\bar{v}\sigma_J)^{-1} \quad (18)$$

Similarly,

$$\tau_{\theta,2} = (\rho\bar{v}\sigma_{\theta,2})^{-1} \quad (19)$$

for quadrupolar relaxation. The experimental thermal average collision cross sections σ_J and $\sigma_{\theta,2}$ are respectively identified with the theoretical averages:

$$\sigma_J = [\mathbf{d}^{(1)}\langle\sigma^{(1)}\rangle^{-1}\mathbf{P}\mathbf{d}^{(1)}]^{-1} \quad (20)$$

$$\sigma_{\theta,2} = [\mathbf{d}^{(2)}\langle\sigma^{(2)}\rangle^{-1}\mathbf{P}\mathbf{d}^{(2)}]^{-1} \quad (21)$$

Thus, T_1 measurements in the extreme narrowing limit provide a temperature-dependent effective collision cross section that has a clearly defined meaning in terms of molecular dynamics and has a well-defined connection to the potential energy surface. Given an intermolecular potential energy surface, calculations of σ_J and $\sigma_{\theta,2}$ by eqs 20 and 21 can be carried out for a particular choice of scattering theory. Some examples are N_2–N_2 by classical scattering,[84] HCl–Ar by semiclassical scattering,[87] and H_2–He, HD–He by close-coupled quantum scattering.[75,76] The latter are discussed in a later section.

B. Changes in the Angular Momentum Vector

When the spin relaxation is completely dominated by either the spin-rotation mechanism, or by the quadrupolar mechanism, then measurements of (T_1/ρ) as a function of temperature for the pure gas establishes the characteristics of the like-molecule collisions. It has been shown theoretically[85] and experimentally,[86,87] that in the extreme narrowing limit the spin rotation or the quadrupolar relaxation time in a mixture is made up of additive contributions from various collision partners

$$T_1 = (T_1/\rho)_{\text{A-A}}\rho_A + (T_1/\rho)_{\text{A-B}}\rho_B \quad (22)$$

provided the gas pressures are low enough such that the effects of successive collisions are not correlated. The characteristic $(T_1/\rho)_{\text{A-B}}$ provides $\sigma_J(T)$ or $\sigma_{\theta,2}(T)$ for the A–B collision pair.

If spin-relaxation measurements of two different spin nuclei on the same molecule are used to determine the σ_J cross sections, as for $^{15}N^{15}NO$,[88] both should lead to the same cross sections since it is the rotational angular momentum vector of the entire molecule that is involved, although the individual nuclear spins make their connections to this vector via different spin rotation tensors. For a spherical top, in the extreme narrowing limit,[89]

$$(1/T_1)_{\text{lin,SR}} = [C^2_{\text{av}} + (4/45)(\Delta C)^2]2I_0kT/\rho\bar{v}\ \sigma_J \quad (23)$$

The isotropic value C_{av} and the anisotropy ΔC in the spin rotation tensor are available from molecular beam magnetic or electric resonance spectroscopy or high-resolution microwave spectroscopy. They can also be obtained from absolute shielding by the identity expressed in eq 10.

Relaxation times have been measured for the ^{19}F nucleus in CF_4, SF_6, SeF_6, TeF_6, ^1H and ^{13}C in CH_4, ^{13}C in CO and CO_2, and ^{15}N in N_2 and NNO molecules in the set of buffer gases Ar, Kr, Xe, N_2, CO, HCl, CO_2, CH_4, CF_4, SF_6, and in some cases NNO, SeF_6, and TeF_6 as well.[86-88,90-95] The cross sections σ_J(300 K) obtained from these measurements are shown in Table IV. An examination of these cross sections reveals the following:[95]

(1) Collision efficiencies can be defined in terms of the collision cross section divided by a geometric cross section, to take into account the relative sizes of the molecules. We have been using $(\sigma_J/\pi d_{12}^2)$, where d_{12} is taken from the distance scaling parameter in the conformal potential functions.[96] The most important factor which determines the absolute magnitude of the observed efficiencies of angular momentum change in the target molecule 1 by collision partner 2 is the anisotropy of the electronic distribution of the target molecule. For any given collision partner, the largest efficiencies are those for NNO molecule followed by CO_2 and CO. To an approaching projectile, the anisotropy of the NNO molecule appears the greatest, followed by CO_2 and CO, in that order. The shape of the projectile molecule is of secondary importance. On a nearly isotropic target molecule such as SF_6, projectiles Ar and HCl have the same effect as do CF_4 and Xe.

(2) The collision cross section for any given observed molecule increases with increasing mass (and number of electrons) of collision partner, not unexpected because of the increase in geometric size. Corrected for the geometric sizes, the collision efficiencies also in-

TABLE IV. Thermal Average Collision Cross Sections for the Change in the Molecular Rotational Angular Momentum Vector, σ_J(300 K) (Å^2)[a]

molecular partner	$^{15}N^{15}NO$	$^{13}CO_2$	^{13}CO	$^{15}N_2$	CF_4	CH_4	SF_6	SeF_6	TeF_6
CH_4	30.8	28.1	19.7	14.2	12.2	18.4	9.1	12.3	17.7
N_2	34.0	26.6	20.8	14.9	12.7	16.3	11.0	14.4	16.4
CO	33.1		22.0	15.0	12.8	15.8	12.0	16.0	18.7
HCl	52.4	53.5	30.2	22.7	22.0	23.7	16.1	24.5	32.7
Ar	37.7	33.9	21.1	15.9	19.2	14.4	16.1	19.4	27.7
CO_2	59.8	59.9	37.1	29.4	29.7	24.1	25.0	33.5	43.3
Kr	55.6	49	26.8	18.1	29.2	18.3	27.0	38.9	47.7
CF_4	71.7	61.6	41.5	30	39.4	24.4	39.6	56.2	66.9
Xe	64.6	62	30.8	19.8	34.3	22.4	34.8	50.4	64.6
SF_6	102.4	91	50.0	38.1	58.0	34.5	64.1	82.2	109.6
NNO	59.3								
SeF_6								105.2	
TeF_6									129.1

[a] From refs 86–88 and 90–95.

TABLE V. Temperature Dependence of the Collision Cross Sections for the Change in the Molecular Rotational Angular Momentum Vector

$$\sigma_J(T) = \sigma_J(300\ \text{K})(T/300)^{-m}$$

molecular partner	m[a]								
	$^{15}N^{15}NO$	$^{13}CO_2$	^{13}CO	$^{15}N_2$	CF_4	CH_4	SF_6	SeF_6	TeF_6
CH_4		0.86		0.60	0.95	0.93	0.99	1.32	1.51
N_2	0.81	0.74	1.12	0.70	0.77		1.07	1.24	1.28
CO	0.81		0.82	0.67	0.74		1.07	1.26	1.37
HCl	1.04	1.1	0.91	0.98	0.88	1.03	0.95	1.24	1.40
Ar	0.86	0.77	0.61	0.74	0.51	1.09	0.97	1.19	1.34
CO_2	0.94	1.01	0.67		1.06	1.10	1.17	1.34	1.61
Kr	0.96	0.85	0.67	0.74	0.93		1.12	1.39	1.37
CF_4	0.87			0.88	0.91	1.09	1.21	1.48	1.33
Xe	0.92	1.1	0.75	0.77	0.97		1.23	1.46	1.53
SF_6		1.1	0.44		0.90		1.25	1.41	1.62
NNO	0.91								
SeF_6								1.47	
TeF_6									1.32

[a] Data taken from refs 86–88 and 90–94.

crease with increasing mass (and number of electrons) of the collision partner. Part of this has to do with the kinematic factors which can be modeled by classical collisions between hard bodies. Chandler's model[97] involves a kinematic factor in the collision efficiency which is of the form[95]

$$\left[\frac{I_1}{\mu_{12}{d_{11}}^2} + \frac{1}{2}\left(1 + \frac{I_1{d_{22}}^2}{I_2{d_{11}}^2}\right)\right]^{-1}$$

which applies to linear or spherical top target molecules and molecular collision partners (not atoms). The other part can be attributed to attractive forces increasing roughly with increasing number of electrons of the partner.

(3) The observed collision efficiencies of the CH_4 molecule is nearly the same for all buffers. The small mass of CH_4 has a leveling effect; it makes the reduced mass of the collision pair nearly the same for all partners.

(4) Electrical moments of the collision partner enhance collision efficiencies by introducing sizeable angle-dependent terms in the intermolecular potential. Thus, HCl as a collision partner has a larger efficiency than expected for its number of electrons. So do CO_2 and NNO which have sizeable electric quadrupole moments.

(5) Despite the similarities of NNO with CO_2 or CO with N_2 in mass, number of electrons, and moments of inertia, there are clear differences in their cross sections. This is an indication of the sensitivity of the $\sigma_J(T)$ cross sections to the details of the anisotropy of the intermolecular potential. These results offer the attractive possibility that *different* angle-dependent terms in the SF_6–CO_2 pair potential can be provided by σ_J = 25 Å^2 for SF_6 molecule in collisions with CO_2 than by σ_J = 91 Å^2 for CO_2 molecule in collisions with SF_6 (for example).

The temperature dependence of $\sigma_J(T)$ seems to fit a power law reasonably well, at least to within experimental error. Thus, in Table V we summarize these data in terms of the values of m, as in

$$\sigma_J(T) = \sigma_J(300\ \text{K})(T/300)^{-m} \quad (24)$$

The interesting trend is that, although the m value is very specific to the collision pair, the m value averaged over all pairs for an observed molecule roughly increases with the well depth averaged over all pairs. This is shown by the plot in Figure 9.[93] This is not inconsistent with Chandler's model in which attractive forces are modeled by an exponential factor $\exp(\epsilon_{12}/kT)$ in the collision efficiencies.[95,98] This trend became apparent when SeF_6 and TeF_6 were included in the studies.[93]

C. Molecular Reorientation

The other cross section which can be obtained from spin relaxation measurements is $\sigma_{\theta,2}$, most conveniently determined from quadrupolar relaxation but is also the

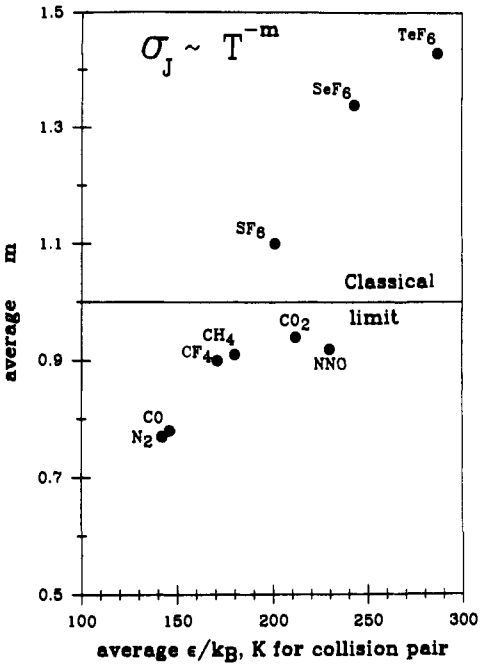

Figure 9. The temperature dependence of the collision cross sections for changes in the rotational angular momentum vector is found to correlate with the average well depth for the collision pair (reprinted from ref 93; copyright 1991 American Chemical Society).

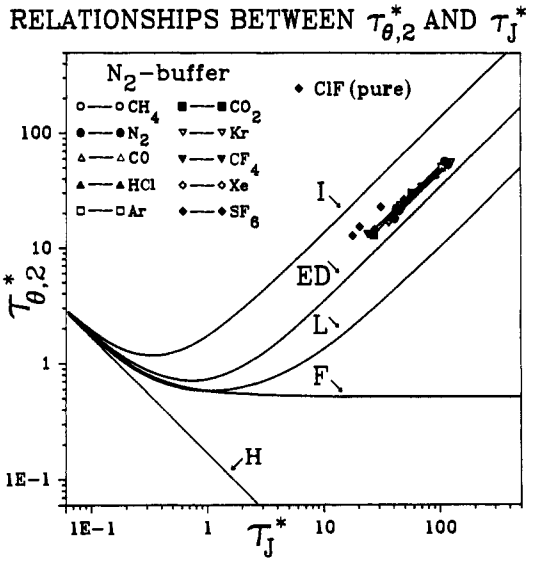

Figure 10. The experimental relationship between the correlation time τ_J for changes in the rotational angular momentum vector and the correlation time $\tau_{\theta,2}$ for molecular reorientation in the gas phase is compared with the predictions of various models for molecular reorientation. The Ivanov, extended diffusion, Langevin, friction, and Hubbard models are described in ref 103 (reprinted from ref 99; copyright 1991 American Institute of Physics).

cross section obtained from intramolecular dipole–dipole relaxation or relaxation by chemical shift anisotropy reorientation. This experimental collision cross section is expressed in terms of Gordon's theory by eq 2. We have undertaken studies of $\sigma_{\theta,2}$ cross sections for two molecules (N_2 and NNO) with the same collision partners in order to gain a better understanding of the relationship between $\sigma_{\theta,2}$ and σ_J. These cross sections are expected to provide complementary information. The spin-rotation mechanism preferentially weights the high j states whereas the quadrupolar mechanism depends primarily on the reorientation of molecules in the low j states.[81] These cross sections are uniquely determined by the intermolecular potential function for the collision pair. Nevertheless, there are some interesting trends which have already been uncovered in σ_J studies and it might be expected that a global view of $\sigma_{\theta,2}$ may emerge from the comparisons in the same set of collision partners.

Both cross sections have been determined for N_2 molecule. The ratio $(\sigma_{\theta,2}/\sigma_J)$ is found to be nearly constant, 2.1 ± 0.2 for N_2 molecule with the 10 collision partners.[99] The ratio $(\sigma_{\theta,2}/\sigma_J)$ for ClF–ClF collisions is 1.38,[100] and for CF_4–CF_4 collisions is very close to 4.0[101] while for CH_4/CD_4 it is 2.94.[94] An examination of $\sigma_{\theta,2} = [\mathbf{d}^{(2)}\langle\sigma^{(2)}\rangle^{-1}\mathbf{P}\mathbf{d}^{(2)}]^{-1}$ and $\sigma_J = [\mathbf{d}^{(1)}\langle\sigma^{(1)}\rangle^{-1}\mathbf{P}\mathbf{d}^{(1)}]^{-1}$ term by term, using the infinite order sudden (IOS) approximation, using Kouri's IOS factorization method,[102] leads to the conclusion that the inequality $(\sigma_{\theta,2}/\sigma_J) > 1.0$ should hold in general.

A further motivation for studies of both cross sections is in differentiating between existing classical theories for molecular reorientation in fluids. These models assume that molecular reorientation can be characterized by correlation times $\tau_{\theta,n}$. The correlation function for the angular momentum vector is similarly characterized in these models by a correlation time τ_J (which is identical with τ_ω in linear and spherical top molecules, i.e., those molecules in which **J** is proportional to the angular velocity ω). As discussed above, in the gas in the extreme narrowing limit, τ_J and $\tau_{\theta,2}$ are well-defined quantities when one uses the impact approximation and assumes uncorrelated binary collisions.

Comparison of $\sigma_{\theta,2}$ and σ_J for N_2 with the predictions of various reorientation models in fluids[103] is shown in Figure 10. These models all predict a *constant* temperature-independent, molecule-independent ratio $(\tau_\omega^*/\tau_{\theta,2}^*)$ in the gas limit, but the values of the constant are 3 (extended diffusion),[104,105] or 3/4 (Ivanov model),[106,107] or 10.05 (Langevin model)[108] for linear molecules, and respectively 4, 4/5, and 24.4 for spherical tops. It is seen that not any of the models gives a good prediction of experiment. Each of the molecular reorientation models predicts a constant $(\sigma_{\theta,2}/\sigma_J)$ ratio for all linear molecules. On the other hand it now appears that a characteristic ratio $(\sigma_{\theta,2}/\sigma_J)$ is obtained for each molecule. For NNO molecule this ratio has been determined in the same set of 10 collision partners as N_2 molecule.[109] While $(\sigma_{\theta,2}/\sigma_J)$ is 2.1 ± 0.2 for N_2, it is 1.3 ± 0.2 for NNO. This poses intriguing questions. Does some fundamental relationship underly the observation of a nearly constant ratio for a molecule irrespective of the collision partner? We now have enough information to make a clear differentiation between the various models. We have observed that the ratio $(\sigma_{\theta,2}/\sigma_J)$ is greater than 1. We find nearly classical behavior in that the ratio is nearly constant for the molecule undergoing reorientation, irrespective of the collision partner. We find a smaller observed ratio (in the range 4/3 to 2) for linear molecules than for spherical tops (3–4). Clearly qualitatively incorrect behavior is predicted by the friction and Hubbard models. The Ivanov model (ratio less than 1) and the Langevin model (larger ratio for linear molecules than spherical tops) also are qualitatively incorrect. The extended diffusion model is most qualitatively consistent with observed data.

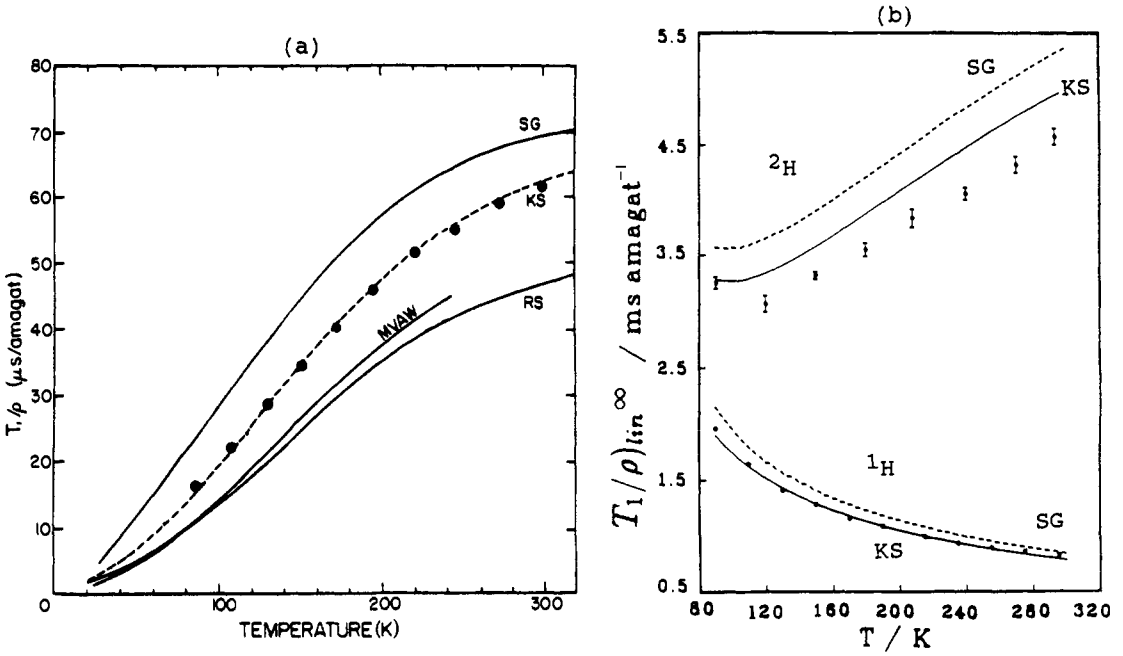

Figure 11. Tests of the H_2–He potential surface: (a) A comparison of T_1 data for H_2 molecule in He with predictions based on several theoretical potentials (labels are explained in the text). (b) The measured relaxation times for the proton and the deuteron in HD molecule in He gas are compared with predictions from two potentials (reprinted from ref 75 and 76; copyrights 1984 and 1990 American Institute of Physics).

D. Tests of Anisotropic Potential Energy Surfaces

There are several potential energy surfaces for the H_2–He system which do not differ significantly in their ability to reproduce various experimental quantities such as virial coefficients, molecular beam scattering, transport properties, and their field effects. These are designated here as MVAW, KS, RS, and SG. The MVAW surface is the ab initio surface of Mulder, van der Avoird, and Wormer,[110] obtained by using a valence-bond approach. The KS surface is based on the full CI ab initio calculations of Meyer et al.[111] refitted with additional Legendre expansion terms by Köhler and Schaefer.[112] RS is a Hartree–Fock plus damped dispersion semiempirical surface obtained by Rodwell and Scoles.[113] SG is an empirical surface fitted to molecular beam scattering, rotational relaxation, and older proton spin relaxation data by Shafer and Gordon.[114,115] Recent spin-relaxation measurements are capable of distinguishing between these surfaces.

In H_2 molecule both spin-rotation and dipolar relaxation mechanisms are important. Thus

$$\left(\frac{\rho}{T_1}\right)_{\text{lin}} = \left(\frac{\rho}{T_1}\right)_{\text{lin,SR}} + \left(\frac{\rho}{T_1}\right)_{\text{lin,d}} \tag{25}$$

For H_2 infinitely dilute in He gas, $(T_1/\rho)^{\infty}_{\text{lin}}$ has been obtained experimentally by extrapolation from a 2% mixture of H_2 in He. The measured temperature dependence of $(\rho/T_1)^{\infty}_{\text{lin}}$ is compared with close-coupled quantum collision calculations of $(\rho/T_1)^{\infty}_{\text{lin,SR}}$ and $(\rho/T_1)^{\infty}_{\text{lin,d}}$ from eqs 11 and 16 by using the various potential surfaces which have been proposed for H_2–He. This comparison is shown in Figure 11a.[75] The same potential energy surface governs the relaxation of both ^1H and ^2D in HD–He. In this case, ^1H relaxes by the spin-rotation and dipolar mechanisms whereas ^2D relaxes by spin-rotation, dipolar, and quadrupolar mechanisms. The comparisons are shown in Figure 11b.[76] It is quite clear that the spin-relaxation data are capable of distinguishing between the surfaces even though other observables such as transport properties and their field effects have not permitted a clear-cut distinction. The proton relaxation which is largely by the spin-rotation mechanism, is completely accounted for by the KS potential surface. The deuteron relaxes primarily by dipolar and quadrupolar mechanisms. As mentioned earlier, these $\sigma^{(2)}$ mechanisms probe slightly different parts of the potential surface than the $\sigma^{(1)}$ mechanism. The sensitivity of the computed spin-relaxation times (and other observables) to different parts of the H_2–He potential has been investigated by Rabitz, McCourt, and co-workers.[115] The route for calculating the observables was from calculation of scattering matrices, to microscopic cross sections, to velocity-averaged cross sections, to effective cross sections (denoted in this review by $\sigma_{\theta,2}$ and σ_J). For each of the terms in the potential function, V_0 (the isotropic part), V_2 (the P_2 (cos θ) term), V_4 (the P_4 (cos θ) term), ... the cross sections show a predominantly negative or predominantly positive response to changes in the potential function, negative for V_0 and V_4, positive for V_2 and V_6. The largest magnitude of these sensitivies is in the repulsive region, below 3 Å. Both $\sigma_{\theta,2}$ and σ_J are found to be very sensitive to V_0 and V_2, sensitive to V_4, and less sensitive to V_6. They note that these observables are very sensitive to the isotropic part of the potential even though the physical phenomenon, spin relaxation by intramolecular mechanisms (spin rotation, dipolar, or quadrupolar), does not exist without the presence of an anisotropy.

In the case of H_2–Ne, a similar comparison as in Figure 11a permitted the adjustment of the preexponential factor in the expression for the repulsive wall of the second Legendre component of the potential by

a mere 3%; this led to changes of the order of 20%–30% in the values of (T_1/ρ) for the proton relaxation.[116] Spin relaxation is the single most powerful test of the anisotropic part of the H_2–rare gas potential surfaces.

There are recent collision calculations (using the IOS approximation) of various properties of N_2–He, –Ne, and –Ar.[117] Many of the surfaces give relatively good agreement with the transport coefficients (diffusion, shear viscosity, thermal conductivity) over an extensive temperature range, but most are unable to predict the cross sections associated with relaxation phenomena (collision broadening of the depolarized Raman and Rayleigh scattering, viscomagnetic effect). Thus, the isotropic part of the potential surfaces are reasonably good but the anisotropies are still inadequate. Multiple property analysis should include the relaxation cross sections σ_J and $\sigma_{\theta,2}$ which are now available for N_2–Ar to yield a realistic characterization of the anisotropy of the N_2–Ar potential surface. It has been established by the H_2–rare gas experiments that σ_J is extremely sensitive to the term $V_2(R)P_2(\cos\theta)$ in the anisotropy. This should be true for N_2–rare gas as well.

E. Spin-Rotation Constants and Absolute Shielding

An interesting application of spin-rotation relaxation studies is the determination of the ^{29}Si absolute shielding scale. By simultaneous T_1 measurements of ^1H and ^{29}Si relaxation in SiH_4 gas, the ratio $C^2_{eff}(^1H)/C^2_{eff}(^{29}Si)$ can be determined.[63] As shown in eq 23 C^2_{eff} is $[C^2_{av} + {}^4/_{45}(\Delta C)^2]$ for a spherical top. The expression for a symmetric top is also well known.[89] Knowing $C^2_{eff}(^1H)$ from molecular beam resonance measurements in SiH_4, one can find $C^2_{eff}(^{29}Si)$ in SiH_4, from which by the use of the connection between the spin-rotation constant and the paramagnetic shielding (eq 10) it is possible to obtain the quantity $\sigma_0(^{29}Si$ in $SiH_4) = 475.3$ ppm. At the same time, in the same gas mixture containing SiH_4 and SiF_4, the concurrent T_1 experiments can be carried out for ^{19}F and ^{29}Si in SiF_4, from which the quantity $\sigma_0(^{29}Si$ in $SiF_4) = 482$ ppm is obtained. An internal check on these two independently obtained values is the measured ^{29}Si chemical shift in the same sample. Thus was the ^{29}Si absolute shielding scale established.[63] With spherical TMS liquid at absolute shielding of 368.5 ppm, all measured ^{29}Si chemical shifts can be converted to the absolute scale. Similarly, the relaxation times of ^{77}Se and ^{19}F concurrently measured in pure SeF_6 gas give the ^{77}Se absolute shielding in SeF_6, and $^{125}Te/^{19}F$ T_1 measurements in pure TeF_6 gas give the ^{125}Te absolute shielding in TeF_6.[118] Effectively, the absolute shielding scales for ^{29}Si, ^{77}Se, and ^{125}Te are based on the well-established ^1H and ^{19}F absolute shielding scales.

It is also possible to derive C^2_{eff} from T_1 measurements through the low-density region of the T_1 minimum. In that region a single relaxation time approximation allows a fit to

$$T_1 = A\rho + B/\rho \qquad (26)$$

A is related to $(\omega_I + \omega_J)/C^2_{eff}\rho_{min}$ and B is related to $(\omega_I - \omega_J)/C^2_{eff}\rho_{min}$, respectively.[89] Recent examples of these studies are the ^1H relaxation in symmetric top benzene[119] and nearly oblate asymmetric top furan.[120]

F. Intermolecular Dipole–Dipole Relaxation

Different theoretical approaches by Chen and Snider,[121] Bloom and Oppenheim,[122] and by Shizgal[123] all lead to the same limiting form for intermolecular dipole–dipole relaxation of spin I by collision partners carrying spin S:

$$\left(\frac{1}{T_1^{DD}}\right)_{\text{theor limit}} = \frac{16}{3}S(S+1)\gamma_I^2\gamma_S^2\left(\frac{\hbar}{d^2}\right)\left(\frac{\pi\mu}{8kT}\right)^{1/2}N_S \qquad (27)$$

In a series of studies of competing relaxation mechanisms in gas mixtures containing oxygen, the nature of the intermolecular dipole–dipole relaxation mechanism has been elucidated.[124–127] By its nature, the dependence of the intermolecular relaxation mechanism on density, temperature, and magnetic field are different from those of the spin-rotation intramolecular mechanism. The separation of the two mechanisms takes advantage of these differences.

In CF_4–O_2 mixtures, for example, with a properly chosen single value of (T_1^{SR}/ρ) at 300 K for the CF_4–O_2 collisions, the remainder, $1/T_1^{DD} = (1/T_1 - 1/T_1^{SR})$ should show a direct proportionality to the density of oxygen at all temperatures and all fields. Indeed, a precise separation was possible for ^{19}F in CF_4 in mixtures containing oxygen in which the relaxation rates range from 10% intermolecular DD/90% SR up to 80% DD/20% SR. Equally precise separation was possible for ^{19}F in SF_6, SeF_6, and TeF_6 in oxygen as well as for ^1H in CH_4 in oxygen.[124,126–128]

The low frequency limit refers to the physical situation in which the nuclear spin-bearing molecule suffers several collisions during one Larmor period. In the low frequency limit, the magnetic field dependence of the intermolecular dipole relaxation can be written in the form:

$$\frac{1}{T_1^{DD}} = \left(\frac{1}{T_1^{DD}}\right)_0\{1 - f(T)\sqrt{\omega_I}\} \qquad (28)$$

Analysis of the data at two or more magnetic fields directly provides the empirical function $f(T)$ without making any assumptions as to the temperature dependence or the functional form of the zero field limit, $(1/T_1^{DD})_0$ or that of $f(T)$, only that $(1/T_1^{DD})_0$ is field independent. With this $f(T)$ function, data at 3 fields and from all samples yield a collision efficiency as a function of temperature. We designate the collision efficiency with the notation $F(V/kT)$ to remind us that it depends on the intermolecular potential. Thus, the equation

$$\frac{1}{T_1^{DD}} = \frac{16}{3}S(S+1)\times \gamma^2\gamma_S^2\frac{\hbar}{d^2}\left(\frac{\pi\mu}{8kT}\right)^{1/2}N_S\cdot F(V/kT)\cdot\{1 - f(T)\sqrt{\omega_I}\} \qquad (29)$$

summarizes the characteristics of the intermolecular dipole–dipole interaction. A magnetic field dependence of T_1^{DD} is observed in these samples at magnetic fields of 1.9–9.4 T because the duration of a collision (during which time CF_4 and O_2 molecules are close enough for

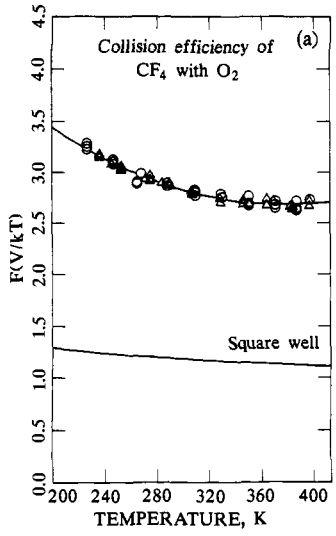

Figure 12. The collision efficiency for intermolecular dipole–dipole spin relaxation in CF_4 molecule with oxygen, obtained from measurements of T_1 for ^{19}F in CF_4 in oxygen gas at three magnetic fields as a function of temperature (reprinted from reference 127; copyright 1991 American Institute of Physics).

the electron spin dipole–nuclear spin dipole to cause nuclear spin transition) is only a tiny fraction (1 part in 10^4) of the Larmor period of the ^{19}F nucleus, but is a sizeable fraction (0.04–0.2) of the Larmor period of the electron spin. The low-frequency limiting form $\{1 - f(T)\sqrt{\omega_I}\}$ appears to be valid since the nuclear-spin-bearing molecule suffers several collisions during one Larmor precession of the electron spin. At yet higher magnetic fields, the terms in ω^2 eventually become important, as is well known from studies in liquids.

The experimental magnetic field dependence has been found to agree quite well with a theoretical expression[127]

$$f(T) = \frac{1}{24}\left(\frac{d_{eff}}{\bar{v}}\right)^{1/2}[3 + 7(\gamma_S/\gamma_I)^{1/2}] \qquad (30)$$

that is based on Abragam's reduced spectral density function, wherein the translation correlation time in liquid models, $\tau_{tr} = d^2/D$, is replaced by the analogous characteristic time in the gas phase, $d_{eff}/\bar{v}$. The experimental effective cross section found in this work is $\pi(d_{eff})^2$, which is expressed in the following form:

$$\pi(d_{eff})^2 = F(V/kT)\cdot\pi r_0^2 \qquad (31)$$

πr_0^2 being the geometric cross section, in which r_0 is obtained from the conformal isotropic intermolecular potentials for the CF_4–O_2 or other collision pair.[96] This theoretical estimate of $f(T)$ agrees quite well with the experimental functions for CH_4, CF_4, SiF_4, SF_6, SeF_6, and TeF_6 with oxygen.[127]

The experimental $F(V/kT)$ functions are fairly well defined for these collision pairs (see for example, Figure 12), and provide an experimental measure of the collision efficiencies for intermolecular dipole–dipole relaxation in these molecules upon collision with oxygen molecule. Values at 300 K are 1.195, 1.296, 1.333, 1.310, 1.383, and 1.392 for CH_4, CF_4, SiF_4, SF_6, SeF_6, and TeF_6 with O_2, respectively. As might be expected, collision efficiencies increase with decreasing temperature in all cases. These efficiencies are greater than the collision efficiencies for spin-rotation relaxation in these molecules with any collision partner. With these studies, the intermolecular dipole–dipole relaxation mechanism has been fully characterized.

In the examples shown here, there are no obvious contributions to the relaxation from the dimer populations, not surprising for O_2 interacting with the molecules studied at these temperatures, even xenon atom. In contrast, the hyperfine interaction of the ^{129}Xe with the unpaired electron in the transient diatomic molecule XeRb does play a role in the ^{129}Xe spin relaxation for xenon in Rb/buffer mixtures and is an important mechanism by which the ^{129}Xe nuclear spin becomes polarized,[129] as well as a means by which the average hyperfine constant for the ^{87}Rb nuclear spin is changed.[130,131] On a more practical side, the intermolecular dipolar mechanism provides an important relaxation mechanism for ^{129}Xe in the presence of even small concentrations of oxygen,[125] which in turn permits much shorter delays between 90° pulses in the acquisition of ^{129}Xe spectra in various applications of xenon NMR in investigations of zeolites and other porous solids.

G. Conclusions

Gas-phase NMR measurements provide two types of collision cross sections σ_J and $\sigma_{\theta,2}$ that have well-defined relationships to the intermolecular potential energy surface. We have seen that these cross sections provide powerful tests of proposed surfaces. The measured temperature dependence of the σ_J cross sections is well described by a power law T^{-m}, but m is not 1 in every case. Indeed m is found to depend on the well depth of the average isotropic potential but is nevertheless unique for a molecule in a collision pair. This is as it should be, for the intimate relationship between the sigma matrices $\langle\sigma^{(1)}\rangle$ and the intermolecular potential surface for the pair cannot be described by a simple correlation. The magnitudes of the cross sections are useful in their own right for researchers interested in dynamics and energy disposal in the gas phase. Our studies provide useful insight into the factors which determine those magnitudes. The relationship between the two types of cross sections also provides tests of various models for molecular reorientation in fluids. Each cross section is a powerful test of the anisotropy of the intermolecular potential function; when given a potential surface the appropriate (classical, semiclassical, or quantum) scattering calculations should yield a temperature-dependent cross section that can be compared with experiment. The intermolecular dipolar mechanism provides yet another glimpse into the intermolecular potential energy surface.

IV. Chemical Reaction Dynamics

NMR spectroscopy has been a very important tool in the studies of rate processes such as conformational equilibria and chemical exchange in solution. Gas-phase NMR studies can provide the same type of information, for example, rate constants as a function of temperature. However, gas-phase studies provide more extensive and more detailed information than can be obtained from condensed-phase experiments. Furthermore, some unimolecular processes which are completely obscured by intermolecular processes in con-

TABLE VI. Gas-Phase Unimolecular Activation Parameters[a]

system	ref	$E_{act(\infty)}$	$\Delta G^{\ddagger}_{298}$	$\Delta H^{\ddagger}_{298}$	$\Delta S^{\ddagger}$	$\Delta G^{\ddagger}_{gas} - \Delta G^{\ddagger}_{liquid}$
cyclohexane	135	12.5	10.2	12.1	5.7	+
trimethylenimine	132		17.9			
N,N-dimethylpiperazine	136	15.2	12.8	14.3	6.1	-
1,3,5-trimethylhexahydropyran	137	13.8	12.4	13.2	2.8	-
tetrahydropyran	138	12.1	10.5	11.6	6.0	+
cyclohexyl fluoride	139	12.2	10.7	11.6	3.3	+
N,N-dimethylfluoracetamide	140	16.7	16.4	16.1	-1.1	-
N,N-dimethylformamide	141	20.5	19.4	19.7	1.0	-
N,N-dimethylacetamide	142	16.5	15.3	15.8	1.5	-
N,N-diethylformamide	143		19.2	19.4	0.8	-
MeONO	144	12.23	11.97	11.74	-0.91	~0
EtONO	145	11.32	11.01	10.86	-0.63	~0
n-PrONO	145		11.22			~0
neo-PentONO	145		11.18			~0

[a] All values are in kcal mol^{-1} except for $\Delta S^{\ddagger}$ which is eu.

densed phase can be studied in the gas.[132]

Gas-phase NMR experiments can provide insight into vibrational dynamics of unimolecular processes such as conformational isomerism, ring inversion, etc., and can provide information about the nature of solvent effects when compared with studies in the liquid phase. Gas-phase studies of reaction dynamics in three different regimes provide a variety of information. In the *unimolecular region* (high-pressure limit) the observed temperature dependence of the unimolecular rate constant k_{uni} gives gas-phase unimolecular activation parameters $\Delta G^{\ddagger}$ $\Delta H^{\ddagger}$, and $\Delta S^{\ddagger}$ such as those shown in Table VI. In the *bimolecular region* (linear pressure region) the linear dependence of k_{uni} on the pressure of the bath gas gives slopes which are a measure of collision efficiencies for intermolecular vibrational energy transfer. The temperature dependence of unimolecular rate constants obtained in the bimolecular region gives the threshold energy E_0 for conformer conversion. In the *zero-pressure limit* the unimolecular rate constant reveals heterogenous contributions, if any, and can reveal the intrinsic rate that an energized molecule in the absence of collisions, undergoes a conformational conversion. This rate is the rate for conversion that would be measured in a molecular beam, which can provide additional information on the nature of the intramolecular vibrational redistribution process.[133]

A. The Unimolecular Region

1. Activation Parameters for Unimolecular Processes

From the temperature-dependent unimolecular rate constants determined in the infinite pressure limit by means of ^{1}H NMR line-shape analysis, one can get activation parameters for the process.[134] In these line-shape analyses the shieldings, spin–spin coupling constants, and natural line widths are assumed to be independent of pressure and temperature. For example, the values of $E_{act}(\infty)$, $\Delta G^{\ddagger}_{298}$, $\Delta H^{\ddagger}_{298}$, $\Delta S^{\ddagger}_{298}$ for ring inversion, for syn–anti conformational change in alkyl nitrites, and for internal rotation in amides that have been derived by True et al.[132,135-145] are shown in Table VI. These activation parameters obtained in the gas phase provide stringent tests for calculations of potential surfaces for isomerization. At the present time, there are not very many such potential surfaces which have been determined, although a large amount of work has been done on the HCN–HNC rearrangement. The magnitudes of the activation parameters for ring inversion, or syn–anti isomerization of amides or nitrites have importance in semiempirical modeling of structure and dynamics of large molecules.

2. Solvent Effects

Direct comparison of gas-phase data with the corresponding data obtained in condensed phase in various solvents provides information on the direction and extent of solvent effects on the kinetic parameters associated with the conformational exchange process. What has been found in several studies by True et al. is that the phase-dependent variations in these parameters correlate with steric requirements of the transition state associated with each process. Packing forces in solution appear to be the dominant factor in determining the change in $\Delta G^{\ddagger}$. In the methyl nitrite system where the two conformations differ in polarity as well as volume, the solvent effects are small, indicating that the two effects may be nearly equal in magnitude and opposite in direction.[144] For ring inversion in cyclohexane[135] and pseudorotation in SF_4[146] the exchange rates observed in the gas are slower by a factor of 2–3 than those observed in solution. These observations are consistent with the twist-boat transition state for cyclohexane occupying a somewhat smaller volume than the chair conformation, and are consistent with the square pyramidal transition state for SF_4 pseudorotation being smaller than the equilibrium configuration. On the other hand, the gas-phase exchange rates for internal rotation in amides are much faster by ca. 25–30 times than in solution.[143] This is consistent with the greater steric requirements of a transition state having free rotation about the C–N bond. Table VI shows the sign of [$\Delta G^{\ddagger}$(gas) - $\Delta G^{\ddagger}$(liq)] for various systems. These provide tests of theories on the effects of liquid packing on conformational structures.[147] The effect of packing forces in the liquid has been estimated by True et al. by considering the steric contribution to the activation volume $\Delta V^{\ddagger}$ for the process, using effective hard sphere diameters for methyl groups etc. and using the volumes occupied by the solids of revolution generated by rotating the groups relative to each other. Such a model appears to account for the phase dependence of $\Delta G^{\ddagger}$ in those cases where polarity differences play a limited or inconsequential role. On the other hand, in keto–enol tautomerism (in acetylacetone, methyl acetoacetate and ethyl acetoacetate), the observation that the keto forms are stabilized by about 2 kcal mol^{-1} in condensed phases relative to the gas phase can be accounted for on the

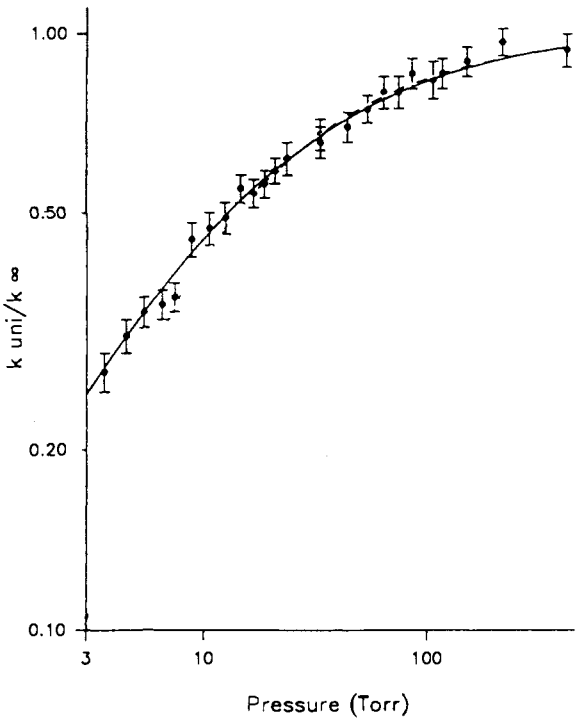

Figure 13. Logarithmic plots of the experimental values of k_{uni}/k_{∞} vs effective pressure for ring inversion of *N*-methylmorpholine in SF_6 gas. The curve represents values obtained from RRKM calculations (reprinted from ref 150; copyright 1990 American Chemical Society).

basis of electrostatic effects which favor the form with the greater dipole moment. The steric factors which would favor the smaller enol form in the condensed phase appear to be much less important than the electrostatic factors.[148]

B. The Bimolecular Region

1. Tests of RRKM Theory

In the Lindemann mechanism for the unimolecular reaction, which may be written as[149]

$$A + M \xrightarrow{k_1} A^* + M$$

$$A^* + M \xrightarrow{k_2} A + M$$

$$A^* \xrightarrow{k_3} A$$

the overall rate of reaction is given by

$$\text{rate} = k_{uni}[A] = k_3[A^*] = \frac{k_1 k_3 [A][M]}{k_2[M] + k_3} \qquad (32)$$

As the pressure is decreased, $k_3 \gg k_2[M]$ and the reaction order changes from first to second.

The bimolecular kinetic region is where a linear pressure dependence is observed in the rate constant k_{uni}. A typical fall-off curve for the experimental rate constants with decreasing pressure of bath gas is shown in Figure 13 for the ring inversion in *N*-methylmorpholine.[150] One of the successes of RRKM theory is in reproducing the experimental fall-off curves of k_{uni} with decreasing pressure in thermal unimolecular reactions with well-defined potential energy barriers.[151] Two important assumptions of RRKM theory are the strong collision assumption and that of rapid intramolecular vibrational energy relaxation. Interpretation of experimental fall-off curves in terms of the RRKM theory makes use of the language inherent in these assumptions. According to the strong collision assumption, large amounts of energy are transferred in individual molecular collisions leading to deactivation or activation. The collisions are assumed to be sufficiently strong so that the distribution of energy resulting from collisions is random. The k_{uni} in this bimolecular regime is the rate at which the molecules are excited to vibrational levels having energy greater than a threshold energy E_0. RRKM theory provides a method of calculation of k_{uni} as a function of pressure.[151] (Programs are available from QCPE.) The required density of states are also calculated by direct count with use of these programs.

RRKM theory predicts that the average rate at which critically energized molecules proceed to become products is inversely proportional to the total density of states of the reacting molecule. The thermal unimolecular reactions which had previously been studied involved threshold energies of >38 kcal mol^{-1}, whereas NMR studies provide information on systems with threshold energies in the 8–20 kcal mol^{-1} range.[150,152-155] The density of vibrational states associated with these moderate threshold energies are much lower (~50 and 15 000 states/cm^{-1}) than the ca. 10^6 associated with the earlier studies on which the successes of RRKM theory have been based. In a series of studies, True et al. have investigated the ability of RRKM theory to model the pressure dependence of the pseudounimolecular rate constant k_{uni} for various processes, including syn–anti conformational change in alkyl nitrites, ring inversion in six-membered rings, and Berry pseudorotation in SF_4.

Gas-phase NMR studies of ring inversion have demonstrated statistical IVR at the following density of states and threshold energies: $N(E^*) \approx 700$ states/cm^{-1} at $E_0 = 12.0$ kcal mol^{-1} in tetrahydropyran,[138] $N(E^*) \approx 1500$ states/cm^{-1} at $E_0 = 12.5$ kcal mol^{-1} in cyclohexane,[135] $N(E^*) \approx 3100$ states/cm^{-1} at $E_0 = 11.5$ kcal mol^{-1} in cyclohexyl fluoride,[139] $N(E^*) \approx 9800$ states/cm^{-1} at $E_0 = 12.2$ kcal mol^{-1} in *N*-methylmorpholine,[150] $N(E^*) \approx 1.3 \times 10^6$ states/cm^{-1} at $E_0 = 14.7$ kcal mol^{-1} in *N*,*N*-dimethylpiperazine,[136] and $N(E^*) \approx 5.9 \times 10^6$ states/cm^{-1} at $E_0 = 13.2$ kcal mol^{-1} in 1,3,5-trimethylhexahydro-1,3,5-triazine.[137] In contrast, the ^{19}F NMR studies of the rate constants for pseudorotation of SF_4 in the gas phase with density of states ca. 60 states/cm^{-1} at $E_0 = 12.7$ kcal mol^{-1} indicate that IVR rates in SF_4 are roughly 2 orders of magnitude slower than that calculated from an RRKM model.

Increasing the chain length from methyl to *n*-butyl in the alkyl nitrites, increases the density of states at the threshold energy by roughly 1 order of magnitude with the addition of each CH_2 group, but these involve parts of the molecule that are increasingly farther removed from the reaction coordinate. The question posed in these studies was whether these states are accessible for the conformational conversion process. Gas-phase dynamic NMR studies by True et al.[153] in this series of molecules showed that in all cases the rates could be fitted by RRKM theory using reasonable values for the parameters. This gives strong support to the conclusion that the IVR in all the alkyl nitrites

is rapid compared to the average rate that critically energized molecules undergo conformational change, i.e., the energy acquired in the additional vibrational states with each added CH_2 group *are* available for the conformational exchange process. RRKM calculations for the alkyl nitrites in CO_2 have been fitted to the fall-off data by using reasonable values for vibrational frequencies and threshold energies derived from measured activation energies, adjusting both the collision diameter σ_{11} and the bath gas efficiency, $[(k_{bi})_{12}/(k_{bi})_{11}]$ separately. With these adjustable parameters, the shape of the k_{uni} vs pressure curve is in good agreement with RRKM calculations.[153]

One important conclusion of these studies is that even systems with sparse density of vibrational states follow RRKM kinetics. Good agreement with RRKM theory in the ring inversion studies[150] and the alkyl nitrite syn–anti conformational exchange kinetics[153] gives strong support to the postulates of the RRKM theory, in particular, the strong collision assumption and the basic assumption that intramolecular vibrational energy redistribution in these systems is rapid and statistical, even at energies at which the vibrational manifold should be reasonably well describable in terms of normal modes. IVR is unusually efficient for molecules with torsional degrees of freedom.[156]

2. Intermolecular Energy Transfer

From the analysis of the pressure-dependent studies in the bimolecular kinetic region where there is a linear pressure dependence to the observed rate constants, collision cross sections for intermolecular energy transfer may be obtained. From the slope of the fall-off curve in k_{uni} vs pressure one obtains the bimolecular rate constant k_1 or k_{bi}. In different bath gases, different values of k_{bi} are obtained. The collision efficiencies of various bath gases relative to the reactant molecule are designated by β_μ, a measure of the relative effectiveness of bath gas molecules compared to reactant molecules in collisions that result in intermolecular energy transfer leading to conformer interconversion:

$$\beta_\mu = \frac{(k_{bi})_{12}}{(k_{bi})_{11}}\left(\frac{\mu_{12}}{\mu_{11}}\right)^{1/2} \quad (33)$$

The reduced mass factor takes into account the relative velocities for the two types of collision partners. Alternatively, in terms of effective cross sections

$$\beta_\mu = \sigma_{12}/\sigma_{11} \quad (34)$$

in which σ_{12} is the *effective cross section* for the reactant molecule–bath gas molecule pair, whereas σ_{11} is the effective cross section for the reactant–reactant molecular pair. It is quite appropriate to define cross sections in a strong collision limit.

For various molecules colliding with cyclohexane in intermolecular energy transfer that leads to cyclohexane ring inversion, the relative efficiencies range from β_μ = 0.18 (He) to 0.485 (C_4F_8), the β_μ of cyclohexane with itself defined as 1.0. These are seen to roughly increase with increasing polarizability of the collision partner in Figure 14.[155] A similar correlation has been found for 15 collision partners in the MeONO exchange.[152] This would seem to indicate that the attractive portion of the intermolecular potential plays a major role in the intermolecular energy transfer. Part of the perceived sharp increase with polarizability must be due to kinematic factors such as the reduced mass of the pair and the geometric size of the collision partner, as has been found in other collision cross sections.

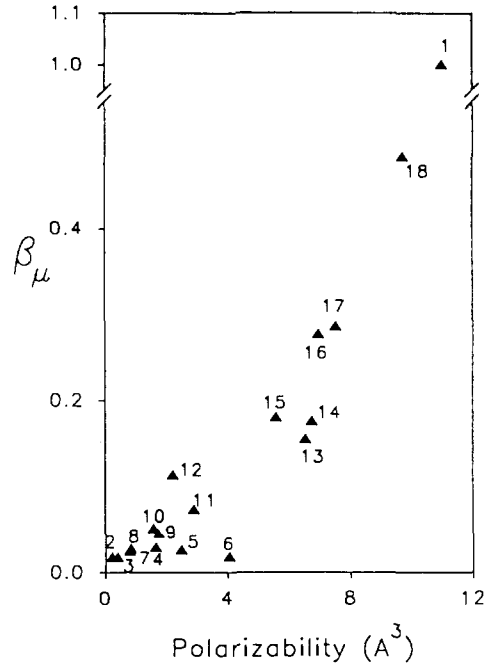

Figure 14. Collision efficiency for intermolecular vibrational energy transfer leading to cyclohexane ring inversion in various gases correlated with the polarizability of the bath gas (reprinted from ref 155; copyright 1991 American Chemical Society).

Extrapolation of k_{uni} at the very low pressure regime to zero pressure should give the same value for cyclohexane in all bath gases, namely the collisionless rate of conformational conversion of an energized molecule. However, due to the intrinsic low sensitivity of NMR spectroscopy and the nonlinear behavior of k_{uni} at pressures below the linear region, the data are not good enough for extrapolation at this limit.

C. Conclusions

Gas-phase NMR spectroscopy has provided extensive and detailed information about unimolecular reactions. The use of pressure as a variable allows the exploration of the unimolecular region and the bimolecular region, permitting the determination of solvent-free activation parameters, threshold energies for bimolecular activation, and tests of RRKM theory. In the examples that have been studied by NMR (ring inversion, syn–anti isomerization, and pseudorotation), it has been found that the results are consistent with RRKM theory, except in the pseudorotation of SF_4, in which non-RRKM behavior was documented. In addition, studies in the bimolecular region have provided collision efficiencies for intermolecular energy transfer. These are understandably very small for rare gases where V–V energy transfer is not possible. Systematic studies of cyclohexane inversion and of methyl nitrite isomerization reveal a correlation of these efficiencies with polarizability of the collision partner or the intermolecular potential well depth, although part of the sharp increase must be due to the accompanying increase in the reduced mass of the collision pair and the geometric size of the collision partner.

V. Conclusions

We have seen that gas-phase NMR spectroscopy provides important information that is otherwise not available. These include collision cross sections for angular momentum vector changes (changes in the **J** vector), for molecular reorientation (changes in the tensor polarization $\mathbf{JJ}/(4\mathbf{J}^2 - 3)$ at low densities), for intermolecular transfer of vibrational energy, and for intermolecular dipole–dipole interaction. By comparison with condensed-phase data, it is possible to deduce solvent effects which are operating on nuclear shielding, and on activation parameters for unimolecular reactions, effects which would not otherwise be separable from the intrinsic quantities of interest when measured in condensed phases. Quantities which are characteristic of isolated molecules or of colliding pairs of molecules can be measured. Tests of various theoretical models are made possible, ranging from high-level ab initio electronic structure and properties, anharmonic intramolecular potential surfaces, intermolecular potential surfaces, molecular scattering calculations, RRKM theory of unimolecular processes, and even rotational diffusion theories in fluids. An understanding of the intermolecular effects on nuclear shielding in the gas phase is essential for the interpretation of various studies of chemical shifts of molecules physisorbed on surfaces or trapped inside porous solids such as zeolites. An understanding of the spin relaxation by the intermolecular nuclear spin dipole–electron spin dipole mechanism is important for the interpretation of the spin relaxation of molecules colliding with Pt or other paramagnetic particles on catalytic supports. The fundamental understanding which comes from NMR studies in the gas phase can be very important in the unraveling of various factors that play a role in condensed phases or heterogeneous systems.

VI. Appendix. Some Experimental Details

A typical preparation of low density samples by N. True's group is described as follows:[152,153]

Modified 12-mm NMR tubes are constructed, consisting of a 3.5-cm portion of a Wilmad high precision 12-mm coaxial inserts with a 5-cm long 3-mm o.d. standard wall Pyrex glass tubing sealed to the end. These modified 12-mm NMR tubes are attached to the vacuum line with $^1/_4$ in. Cajon ultraTorr fittings with $^1/_8$ in. ultraTorr adaptors. The NMR tubes, the vacuum line and lecture bottle connections are evacuated to a pressure <1 mTorr for at least 12 h prior to sample preparation. Pressures between 100 mTorr and 1000 Torr are measured with an MKS Baratron capacitance manometer. TMS is first introduced into the vacuum line and NMR tube, followed by the introduction of the gases of interest. A period of 15 min is allowed for diffusional mixing, after which the NMR tube is quickly sealed with a torch followed by immersion in liquid nitrogen.

Spectra are taken running in unlocked mode on nonspinning samples in a standard 12-mm proton probe. In a wide-bore magnet, 20-mm NMR tubes can be used, or the modified 12-mm NMR tubes are held in a specially manufactured Teflon adapter (12 mm i.d., 20 mm o.d.) which is itself held in a 20-mm spinner. Each sample is allowed 15 min to achieve thermal equilibrium. Nonspinning samples afford better temperature control. Temperatures are calibrated by using four copper constantan thermocouples placed at 1-cm intervals in an empty sample tube, and temperatures are regulated to 0.1 °C. The number of transients collected depends greatly on the sample. For proton NMR (at 300 MHZ) of alkyl nitrites, 2000 transients produced exchange-broadened spectra with S/N ratios greater than 35/1.

VII. References

(1) Govil, G. *Appl. Spectrosc. Rev.* **1973**, *7*, 47.
(2) Jameson, C. J. *Bull. Magn. Reson.* **1980**, *3*, 3.
(3) Armstrong, R. L. *Magn. Reson. Rev.* **1987**, *12*, 91.
(4) Jameson, C. J.; Gutowsky, H. S. *J. Chem. Phys.* **1964**, *40*, 1714.
(5) Jameson, C. J.; Mason, J. In *Multinuclear NMR*; Mason, J., Ed.; Plenum Press: New York, 1987; p 51.
(6) Buckingham, A. D.; Pople, J. A. *Faraday Soc. Discuss.* **1956**, *22*, 17.
(7) Jameson, C. J.; Jameson, A. K.; Oppusunggu, D.; Wille, S. *J. Chem. Phys.* **1982**, *76*, 152.
(8) Jameson, C. J.; Jameson, A. K.; Oppusunggu, D. *J. Chem. Phys.* **1984**, *81*, 2571.
(9) Jameson, C. J.; Jameson, A. K.; Cohen, S. M. *J. Chem. Phys.* **1977**, *67*, 2771.
(10) Jameson, C. J.; Jameson, A. K.; Parker, H. *J. Chem. Phys.* **1979**, *70*, 5916.
(11) Jameson, C. J.; Jameson, A. K. *J. Chem. Phys.* **1984**, *81*, 1198.
(12) Jameson, C. J.; Jameson, A. K. *J. Chem. Phys.* **1978**, *69*, 1655.
(13) Jameson, C. J.; Jameson, A. K.; Oppusunggu, D. *J Chem. Phys.* **1984**, *81*, 85.
(14) Jameson, C. J.; Jameson, A. K. *J. Magn. Reson.* **1985**, *62*, 209.
(15) Jameson, C. J.; Jameson, A. K.; Oppusunggu, D. *J. Chem. Phys.* **1984**, *81*, 2313.
(16) Jameson, C. J.; Jameson, A. K.; Wille, S. *J. Chem. Phys.* **1981**, *74*, 1613.
(17) Jameson, C. J.; Jameson, A. K.; Oppusunggu, D. *J. Chem. Phys.* **1986**, *85*, 5480.
(18) Jameson, A. K.; Jameson, C. J.; Gutowsky, H. S. *J. Chem. Phys.* **1970**, *53*, 2310.
(19) Jameson, C. J.; Jameson, A. K.; Cohen, S. M. *J. Chem. Phys.* **1973**, *59*, 4540.
(20) Jameson, C. J.; Jameson, A. K.; Cohen, S. M. *J. Chem. Phys.* **1975**, *62*, 4224.
(21) Jameson, C. J.; Jameson, A. K.; Cohen, S. M. *J. Chem. Phys.* **1976**, *65*, 3401.
(22) Jameson, C. J.; Jameson, A. K.; Parker, H. *J. Chem. Phys.* **1978**, *68*, 3943.
(23) Jameson, C. J.; Jameson, A. K.; Cohen, S. M. *J. Chem. Phys.* **1977**, *66*, 5226.
(24) Smith, A.; Raynes, W. T. *J. Cryst. Spectrosc. Res.* **1983**, *13*, 77.
(25) Jameson, A. K.; Schuett, K.; Jameson, C. J.; Cohen, S. M.; Parker, H. *J. Chem. Phys.* **1977**, *67*, 2821.
(26) Beckett, J. R.; Carr, H. Y. *Phys. Rev. A* **1981**, *24*, 144.
(27) Raynes, W. T.; Buckingham, A. D.; Bernstein, H. J. *J. Chem. Phys.* **1962**, *36*, 3481.
(28) Rummens, F. H. A.; Bernstein, H. J. *J. Chem. Phys.* **1965**, *43*, 2971.
(29) Rummens, F. H. A.; Raynes, W. T.; Bernstein, H. J. *J. Phys. Chem.* **1968**, *72*, 2111.
(30) Jameson, C. J. *J. Chem. Phys.* **1975**, *63*, 5296.
(31) Jackowski, K.; Raynes, W. T.; Sadlej, A. J. *Chem. Phys. Lett.* **1978**, *54*, 128.
(32) Riley, J. P.; Hillier, I. H.; Raynes, W. T. *Mol. Phys.* **1979**, *38*, 353.
(33) Sadlej, A. J.; Zaucer, M.; Azman, A. *Mol. Phys.* **1978**, *35*, 1397.
(34) Schindler, M.; Kutzelnigg, W. *J. Chem. Phys.* **1982**, *76*, 1919.
(35) Grayce, C. J.; Harris, R. A. *Mol. Phys.* **1991**, *72*, 523; **1990**, *71*, 1.
(36) Rummens, F. H. A.; Mourits, F. M. *Can. J. Chem.* **1977**, *55*, 3021.
(37) (a) Jameson, C. J.; Jameson, A. K. *J. Chem. Phys.* **1986**, *85*, 5484. (b) Chesnut, D. B.; Foley, C. K. *Chem. Phys.* **1986**, *110*, 415. (c) Ditchfield, R. *Chem. Phys.* **1981**, *63*, 185.
(38) Jameson, C. J.; Jameson, A. K.; Wille, S.; Burrell, P. M. *J. Chem. Phys.* **1981**, *74*, 853.
(39) Jameson, C. J. *J. Chem. Phys.* **1977**, *66*, 4977.
(40) Jameson, C. J. *J. Chem. Phys.* **1977**, *67*, 2814.
(41) Jameson, C. J. In *Theoretical Models of Chemical Bonding*; Maksic, Z. B., Ed.; Springer-Verlag: Berlin, 1991; Part 3, pp 457–519.
(42) (a) Jameson, C. J.; Osten, H.-J. *Ann. Rep. NMR Spectrosc.* **1986**, *17*, 1. (b) Lazzeretti, P.; Zanasi, R.; Sadlej, A. J.;

Raynes, W. T. *Mol. Phys.* **1987**, *62*, 605. (c) Fowler, P. W.; Riley, G.; Raynes, W. T. *Mol. Phys.* **1981**, *42*, 1463.
(43) Jameson, C. J.; de Dios, A. C.; Jameson, A. K. *J. Chem. Phys.* **1991**, *95*, 1069.
(44) Hansen, A. E.; Bouman, T. D. *J. Chem. Phys.* **1985**, *82*, 5035.
(45) Spirko, V. *J. Mol. Spectrosc.* **1983**, *101*, 30.
(46) Spirko, V.; Stone, J. M. R.; Papousek, D. *J. Mol. Spectrosc.* **1976**, *60*, 159.
(47) Wasylishen, R. E.; Friedrich, J. O. *Can. J. Chem.* **1987**, *65*, 2238.
(48) Gierke, T. D.; Flygare, W. H. *J. Am. Chem. Soc.* **1972**, *94*, 7277.
(49) Jameson, A. K.; Jameson, C. J. *Chem. Phys. Lett.* **1987**, *134*, 461.
(50) Jameson, C. J.; Jameson, A. K.; Burrell, P. M. *J. Chem. Phys.* **1980**, *73*, 6013.
(51) Jameson, C. J.; Jameson, A. K.; Oppusunggu, D.; Wille, S.; Burrell, P. M.; Mason, J. *J. Chem. Phys.* **1981**, *74*, 81.
(52) Jameson, C. J.; Jameson, A. K.; Honarbakhsh, J. *J. Chem. Phys.* **1984**, *81*, 5266.
(53) Jameson, C. J.; de Dios, A.; Jameson, A. K. *Chem. Phys. Lett.* **1990**, *167*, 575.
(54) Chauvel, J. P.; True, N. S. *Chem. Phys.* **1985**, *95*, 435.
(55) Chauvel, J. P.; Folkendt, M. M.; True, N. S. *Magn. Reson. Chem.* **1987**, *25*, 101.
(56) Suarez, C.; True, N. S.; Weiss-Lopez, B. E. *Bol. Soc. Chil. Quim.* **1989**, *34*, 15.
(57) Schindler, M.; Kutzelnigg, W. *Mol. Phys.* **1983**, *48*, 781.
(58) Bouman, T. D.; Hansen, A. E. Presented at The Danish Chemical Society Meeting, Odense, June 1991.
(59) Oddershede, J.; Geertsen, J. *J. Chem. Phys.* **1990**, *92*, 6036.
(60) Wasylishen, R. E.; Connor, C.; Friedrich, J. O. *Can. J. Chem.* **1984**, *62*, 981.
(61) Schindler, M. *J. Chem. Phys.* **1988**, *88*, 7638.
(62) Flament, J. P.; Gervais, H. P.; Rerat, M. *J. Mol. Struct. (THEOCHEM)* **1988**, *41*, 121.
(63) Jameson, C. J.; Jameson, A. K. *Chem. Phys. Lett.* **1988**, *149*, 300.
(64) Fleischer, U.; Schindler, M.; Kutzelnigg, W. *J. Chem. Phys.* **1987**, *86*, 6337.
(65) Bouman, T. D.; Hansen, A. E. *Chem. Phys. Lett.* **1990**, *175*, 292.
(66) Kutzelnigg, W.; Fleischer, U.; Schindler, M. In *NMR Basic Principles and Progress*; Diehl, P., Fluck, E., Kosfeld, R., Eds.; Springer-Verlag: Berlin, 1991.
(67) Fleischer, U.; Schindler, M. *Chem. Phys.* **1988**, *120*, 103.
(68) Jameson, C. J. *Nucl. Magn. Reson.* **1991**, *20*, 1 and previous volumes.
(69) Fowler, P. W.; Raynes, W. T. *Mol. Phys.* **1981**, *43*, 65.
(70) Raynes, W. T.; Fowler, P. W.; Lazzeretti, P.; Zanasi, R.; Grayson, M. *Mol. Phys.* **1988**, *64*, 143.
(71) Paidarova, I.; Komasa, J.; Oddershede, J. *Mol. Phys.* **1991**, *72*, 559.
(72) Hinderman, D. K.; Cornwell, C. D. *J. Chem. Phys.* **1968**, *48*, 4148.
(73) Jameson, C. J.; de Dios, A.; Jameson, A. K. *J. Chem. Phys.* **1991**, *95*, 1069.
(74) Duncan, T. M. *A Compilation of Chemical Shift Anisotropies*; Farragut Press: Madison, 1990.
(75) Lemaire, C.; Armstrong, R. L.; McCourt, F. R. *J. Chem. Phys.* **1984**, *81*, 5275.
(76) Wagner, R. S.; Armstrong, R. L.; Bissonnette, E. C.; McCourt, F. R. W. *J. Chem. Phys.* **1990**, *92*, 5907.
(77) Beenakker, J. J. M.; Knaap, H. F. P.; Sanctuary, B. C. In *Transport Phenomena.*; Kestin, J., Ed.; American Institute of Physics: New York, 1973; p 21.
(78) Wofford, B. A.; Jackson, M. W.; Lieb, S. G.; Bevan, J. W. *J. Chem. Phys.* **1988**, *89*, 2775.
(79) Gordon, R. G. *J. Chem. Phys.* **1966**, *45*, 1649.
(80) Gordon, R. G. *Adv. Magn. Reson.* **1968**, *3*, 1.
(81) Neilsen, W. B.; Gordon, R. G. *J. Chem. Phys.* **1973**, *58*, 4131, 4149.
(82) Liu, W.-K.; McCourt, F. R. *Chem. Phys.* **1978**, *27*, 281.
(83) Bloom, M.; Oppenheim, I. *Can. J. Phys.* **1963**, *14*, 1583. Bloom, M.; Bridges, F. B.; Hardy, W. N. *Can. J. Phys.* **1967**, *45*, 3533.
(84) Turfa, A. F.; Connor, J. N. L.; Thijsse, B. J.; Beenakker, J. J. M. *Physica A* **1985**, *129*, 439.
(85) Gordon, R. G. *J. Chem. Phys.* **1966**, *44*, 228.
(86) Jameson, C. J.; Jameson, A. K.; Buchi, K. *J. Chem. Phys.* **1986**, *85*, 697.
(87) Jameson, C. J.; Jameson, A. K.; Smith, N. C.; Jackowski, K. *J. Chem. Phys.* **1987**, *86*, 2717.
(88) Jameson, C. J.; Jameson, A. K.; Hwang, J. K.; Smith, N. C. *J. Chem. Phys.* **1988**, *89*, 5642.
(89) Courtney, J. A.; Armstrong, R. L. *Can. J. Phys.* **1972**, *50*, 1252.
(90) Jameson, C. J.; Jameson, A. K.; Smith, N. C. *J. Chem. Phys.* **1987**, *86*, 6833.
(91) Jameson, C. J.; Jameson, A. K. *J. Chem. Phys.* **1988**, *89*, 866.
(92) Jameson, C. J.; Jameson, A. K. *J. Chem. Phys.* **1988**, *88*, 7448.
(93) Jameson, C. J.; Jameson, A. K.; Terry, R. *J. Phys. Chem.* **1991**, *95*, 2982.
(94) Jameson, C. J.; Jameson, A. K.; Smith, N. C.; Hwang, J. K.; Zia, T. *J. Phys. Chem.* **1991**, *95*, 1092.
(95) Jameson, C. J.; Jameson, A. K. *J. Chem. Phys.* **1990**, *93*, 3237.
(96) Maitland, G. C.; Rigby, M.; Smith, E. B.; Wakeham, W. A. *Intermolecular Forces, their Origin and Determination*; Clarendon Press: Oxford, 1981; Table A 3.2.
(97) Chandler, D. *J. Chem. Phys.* **1974**, *60*, 3500, 3508.
(98) Andersen, H. C.; Chandler, D.; Weeks, J. D. *Adv. Chem. Phys.* **1976**, *34*, 105.
(99) Jameson, C. J.; Jameson, A. K.; ter Horst, M. A. *J. Chem. Phys.* **1991**, *95*, in press.
(100) Gillen, K. T.; Douglass, D. C.; Griffiths, J. E. *J. Chem. Phys.* **1978**, *69*, 461.
(101) Campbell, J. H.; Seymour, S. J.; Jonas, J. *J. Chem. Phys.* **1973**, *59*, 4151.
(102) Kouri, D. J. *J. Chem. Phys.* **1978**, *69*, 4999.
(103) Powles, J. G.; Rickayzen, G. *Mol. Phys.* **1977**, *33*, 1207.
(104) Gordon, R. G. *J. Chem. Phys.* **1966**, *44*, 1830.
(105) McClung, R. E. D. *J. Chem. Phys.* **1969**, *51*, 3842.
(106) Ivanov, E. N. *Zh. Eksp. teor. Fiz.* **1963**, *45*, 1509.
(107) Kluk, E.; Chrzeszczyk, A. *Acta Phys. Pol. A* **1963**, *44*, 409.
(108) Fixman, M.; Rider, K. *J. Chem. Phys.* **1969**, *51*, 2425.
(109) Jameson, C. J.; Jameson, A. K.; ter Horst, M. A. To be published.
(110) Mulder, F.; van der Avoird, A.; Wormer, P. E. S. *Mol. Phys.* **1979**, *37*, 159.
(111) Meyer, W.; Hariharan, P. C.; Kutzelnigg, W. *J. Chem. Phys.* **1980**, *73*, 1880.
(112) Schaefer, J.; Köhler, W. E. *Physica A* **1985**, *129*, 469.
(113) Rodwell, W. R.; Scoles, G. *J. Phys. Chem.* **1982**, *86*, 1053.
(114) Shafer, R.; Gordon, R. G. *J. Chem. Phys.* **1973**, *58*, 5422. Green, S. *Physica* **1974**, *76*, 609.
(115) Smith, M. J.; Shi, S.; Rabitz, H.; McCourt, F. R. W. *J. Chem. Phys.* **1991**, *94*, 7125.
(116) Wagner, R. S.; Armstrong, R. L.; LeMaire, C.; McCourt, F. R. *J. Chem. Phys.* **1986**, *84*, 1137.
(117) Corey, G. C.; McCourt, F. R. W.; Chapman, S. *Mol. Phys.* **1987**, *62*, 897.
(118) Jameson, C. J.; Jameson, A. K. *Chem. Phys. Lett.* **1987**, *135*, 254.
(119) Folkendt, M. M.; Weiss-Lopez, B. E.; True, N. S. *J. Phys. Chem.* **1988**, *92*, 4859.
(120) Weiss-Lopez, B. E.; Winegar, E. D.; True, N. S. *J. Phys. Chem.* **1988**, *92*, 4052.
(121) Chen, F. M.; Snider, R. F. *J. Chem. Phys.* **1967**, *46*, 3937.
(122) Oppenheim, I.; Bloom, M. *Can. J. Phys.* **1961**, *39*, 845.
(123) Shizgal, B. *Can. J. Phys.* **1976**, *54*, 164.
(124) Jameson, C. J.; Jameson, A. K.; Hwang, J. K.; Dabkowski, D. *J. Phys. Chem.* **1988**, *92*, 5937.
(125) Jameson, C. J.; Jameson, A. K.; Hwang, J. K. *J. Chem. Phys.* **1988**, *89*, 4074.
(126) Jameson, C. J.; Jameson, A. K.; Hwang, J. K. *J. Phys. Chem.* **1989**, *93*, 634.
(127) Jameson, C. J.; Jameson, A. K.; Hwang, J. K. *J. Chem. Phys.* **1991**, *94*, 172.
(128) Jameson, C. J.; Jameson, A. K.; Hwang, J. K.; Terry, R. To be published.
(129) Knize, R. J.; Wu, Z.; Happer, W. *Adv. Atom. Mol. Phys.* **1989**, *24*, 223.
(130) Bender, P. L. Beaty, E. C.; Chi, A. R. *Phys. Rev. Lett.* **1958**, *1*, 311.
(131) Bernheim, R. *Optical Pumping*, Benjamin: New York, 1965.
(132) Friedman, B. R.; Chauvel, J. P.; True, N. S. *J. Am. Chem. Soc.* **1984**, *106*, 7638.
(133) Berne, B. J. *Chem. Phys. Lett.* **1984**, *107*, 131.
(134) Stephenson, D. S.; Binsch, G. Program 365 (DNMR5), *Quantum Chemistry Program Exchange*, Indiana University: Bloomington, IN 47405.
(135) Ross, B. D.; True, N. S. *J. Am. Chem. Soc.* **1983**, *105*, 4871.
(136) LeMaster, C. B.; LeMaster, C. L.; Suarez, C.; Tafazzoli, M.; True, N. S. *J. Phys. Chem.* **1989**, *93*, 3993.
(137) LeMaster, C. B.; LeMaster, C. L.; Tafazzoli, M.; Suarez, C.; True, N. S. *J. Phys. Chem.* **1988**, *92*, 5933.
(138) Chu, P. S.; True, N. S. *J. Phys. Chem.* **1985**, *89*, 2625.
(139) Chu, P. S.; True, N. S. *J. Phys. Chem.* **1985**, *89*, 5613.
(140) Ross, B. D.; True, N. S.; Decker, D. L. *J. Phys. Chem.* **1983**, *87*, 89.
(141) Ross, B. D.; True, N. S. *J. Am. Chem. Soc.* **1984**, *106*, 2451.
(142) Ross, B. D.; True, N. S.; Matson, G. B. *J. Phys. Chem.* **1984**, *88*, 2675.
(143) LeMaster, C. B.; True, N. S. *J. Phys. Chem.* **1989**, *93*, 1307.
(144) Chauvel, J. P.; True, N. S. *J. Chem. Phys.* **1984**, *80*, 3561.

(145) Conboy, C. B.; Chauvel, J. P.; True, N. S. *J. Phys. Chem.* **1986**, *90*, 4388.
(146) Spring, C. A.; True, N. S. *J. Am. Chem. Soc.* **1983**, *105*, 7231.
(147) Pratt, L. R.; Hsu, C. S.; Chandler, D. *J. Chem. Phys.* **1978**, *68*, 4202.
(148) Folkendt, M. M.; Weiss-Lopez, B. E.; Chauvel, J. P.; True, N. S. *J. Phys. Chem.* **1985**, *89*, 3347.
(149) Robinson, P. J.; Holbrook, K. A. *Unimolecular Reactions*; Wiley Interscience: New York, 1972.
(150) LeMaster, C. B.; LeMaster, C. L.; Tafazzoli, M.; True, N. S. *J. Phys. Chem.* **1990**, *94*, 3461.
(151) Hase, W. L. In *Dynamics of Molecular Collisions*, Miller, W. H., Ed.; Plenum Press: New York, 1976; p 121.
(152) Chauvel, J. P.; Friedman, B. R.; Hoa, V.; Winegar, E. D.; True, N. S. *J. Phys. Chem.* **1985**, *82*, 3996.
(153) Moreno, P. O.; LeMaster, C. B.; True, N. S. *J. Phys. Chem.* **1990**, *94*, 8780.
(154) Chauvel, J. P.; Friedman, B. R.; True, N. S. *J. Chem. Phys.* **1986**, *84*, 6218.
(155) Moreno, P. O.; True, N. S. *J. Phys. Chem.* **1991**, *95*, 57.
(156) Longfellow, R. J.; Parmenter, C. S. *J. Chem. Soc., Faraday Trans. 2* **1988**, *84*, 1499.